運輸省港湾技術研究所 (30th Anniversary Issue)

港湾技術研究所報告

REPORT OF THE PORT AND HARBOUR RESEARCH INSTITUTE

MINISTRY OF TRANSPORT

VOL. 31 NO. 5 MAR. 1993

NAGASE, YOKOSUKA, JAPAN

運輸省港湾技術研究所 図書室 蔵書

港湾技術研究所報告 (REPORT OF P.H.R.I.)

第31巻　第5号 (Vol. 31, No. 5) 1993年 3月 (Mar. 1993)

目　次 (CONTENTS)

REPORT OF THE PORT AND
HARBOUR RESEARCH INSTITUTE
Vol. 31, No. 5 (Mar. 1993)

12. Fluidity Characteristics of Muddy Slurry with Compressed Air in Horizontal Pipe

Yoshikuni OKAYAMA
Takeyuki FUJIMOTO
Motokazu AYUGAI
Makoto SUZUKI
Hiroya FUKUMOTO

Synopsis

In recent activities in port and harbor construction works, many efforts have been made to facilitate pipeline transport of high-density dredged soft mud using compressed air. The compressed air seduces the pressure head loss in a pipeline and makes it possible to transport the muddy slurry while maintaining its density at a high level.

Separation of the compressed air from muddy slurry in a reclamation area is extremely easy and the water content of the muddy slurry is very low so the necessary volume of reclamation area can be reduced to a minimum. The amount of spill water from the reclamation area is small, so environment problems do not emerge. This system has a possibility of greatly reducing the overall cost currently associated with conventional reclamation.

However, the compressed air mixed slurry transport systems are now designed based on experiences in the past. It is strongly required to establish the method for designing the muddy slurry transportation system.

Therefore, we carried out laboratory tests to clarify the fluidity characteristics of muddy slurry with compressed air and we succeeded in simulating the flow and in estimating the pressure loss through a pipeline. In the simulation, we use a flow model in which the flow is composed of perfectly separated air and mud.

To demonstrate the simulation and estimation method, we carried out field tests on systems in Mie and Kumamoto reclamation area. The measured pressures are always vibrating. We obtained the portions of air-mud mixed slug through the pipelines from the pressure vibrations.

Applying the developed method to the field tests, we found that the actual measured pressures corresponded with the estimated pressures derived from the method.

Key Words: Non-Newtonian Fluid, Slurry with Compressed Air, Slurry Transport with Compressed Air, High Density Slurry Transport, Dredging and Reclamation

港湾技術研究所報告
第31巻 第5号 (1993. 3)

12. 水平管における空気混入軟泥の流動特性

岡山義邦*・藤本健幸**・鮎貝基和***
鈴木誠***・福本裕哉***

要旨

最近の港湾工事においては，通常の浚渫ポンプでの排送が困難であると考えられるような流動性の極めて低い高濃度の軟泥輸送に対して，空気を混入した状態で輸送する試みが数多く見られる。これは，圧縮空気を混入することによって見かけ上の管内流動抵抗を下げ，しかも軟泥スラリの濃度を高いままで輸送し得るという利点を持った輸送工法であり，従来加水によって高濃度軟泥の流動特性を低下させていた方法と大きく異なっている。

埋め立て地あるいは土砂処分場における空気と軟泥固液スラリとの分離は極めて容易であるため，浚渫土砂の処分地の容量は必要最小限度に抑えられ，この結果埋立地あるいは土砂処分場における排水処分量が減少することになる。すなわち，従来の埋立や土砂処分に伴う総合的コストを大きく引き下げる可能性を持った工法である。

しかしながら，現在各地で試行されている空気混入スラリ輸送システムの設計は，過去の実績あるいは経験に依存する面が多々あり，経済性を評価するためにも適切な流送設計の手法の確立が求められている状況にあるといえる。そこで，施工条件に沿った空気混入スラリの流動を適切に比較検討するための基礎資料として，軟泥スラリ単独の水平管における流動特性ならびに空気を混入した場合の軟泥の流動特性の変化を室内流送実験結果をもとに明らかにした。

さらに，室内実験で明らかにした結果を現地施工データによって検証し，的確な現地規模における管内の流動状況の予測，あるいは効率や経済性を考慮した適切な輸送システムの評価，設計を可能とする手法について検討した。

キーワード：非ニュートン流体，空気混入スラリ，空気圧送，高濃度輸送，浚渫埋立

* 第二港湾建設局 横浜機械整備事務所所長（前 機械技術部 浚渫埋立研究室長）
** 機械技術部 浚渫埋立研究室長
*** 機械技術部 浚渫埋立研究室

Contents

1. Introduction

For slurry transport using mixed air, various methods have been utilized mainly for civil engineering works on land and at sea, including air lift method for large water depth[1],[2], transport of foam soils by pumping in shield work[3],[4], transport of muck by wind force[5], and dredging works using various pneumatic pumps[6].

Also, studies on the flow of three-phases of gaseous, solid and liquid where the solid-liquid slurry itself behaves as Non-Newtonian fluid are being carried out in the areas of chemical industry and food industry[7],[8].

With these research achievements and records as background, high-density muddy slurry with extremely low fluidity has frequently been handled during port construction works in recent years. The transport of this kind of muddy slurry by ordinary dredging pump was conventionally considered to be very difficult. To overcome this difficulty, trial runs using mixed air have been made in many cases. This transport method is advantageous in that the apparent pressure gradient in pipe is reduced by mixing in compressed air and the transport is possible while the density of the muddy slurry is held at a high level; this method is greatly different from the conventional method in which the fluidity characteristics of high-density muddy slurry were lowered by adding water.

Separation of air from the muddy slurry in the reclamation area is extremely easy, so that the volume of dredged sediment in a reclamation area can be reduced to a minimum. In consequence, the amount of excess water to be treated at the reclamation area can be reduced. In short, this method has a possibility of greatly reducing the overall cost normally associated with conventional reclamation.

However, the compressed air mixed slurry transport systems being tried at various places are now often designed based on experiences in the past. It is now strongly required to establish an adequate method for designing muddy slurry transportation system even for the purpose of evaluating its economy.

Therefore, we clarified the changes between the fluidity characteristics of muddy slurry alone in the horizontal pipe and the fluidity characteristics of muddy slurry with compressed air mixed based on the results of laboratory experiments on muddy slurry transportation in order to obtain the basic data for making a comparative review on the fluidity of muddy slurry mixed with air in conformity with the site conditions for works.

Moreover, the results clarified by the laboratory experiments[9] were verified using field data from construction works, and we predicted the situation of fluidity in pipe at the appropriate field scale and reviewed the method which will be able to realize the evaluation and design of a proper transport system in consideration of both efficiency and economy.

2. Laboratory Fluidity Experiment Equipment and Air Pressured Plant in the Field

2.1 Laboratory Fluidity Experiment Equipment and Experiment Methods

The solid-liquid slurry adjusted to a constant density in the slurry tank is sent to a solid-liquid slurry measuring portion and air mixing portion through a slurry pump. Thereafter, the slurry passes the gaseous, solid, liquid, three-phase flow measuring

portion comprising a horizontal pipe and reaches the outlet of the pipe. The slurry containing air is released to the atmosphere, that is, the inlet to tank, and slurry is recovered to the tank again after the separation of gaseous phase. Outline of the whole of the fluidity experiment equipment comprising loop arrangement is shown in **Fig. 1.**

The pressure loss measuring portion is a transparent acrylic pipe 4 m long and 82 mm in inside diameter. Two of the above are used at the front and rear of the air blowing portion. That is, even in the state where air is mixed, the fluidity state of solid-liquid slurry containing no air under the same transport conditions can be observed and measured at the same time. Density of solid-liquid slurry during experiment is obtained from materials sampled in the tank.

Also, the mean void ratio within the horizontal pipe mixed with air was determined by measuring the liquid surface level in the tank. Moreover, as a trial, we determined the absolute velocity of air slug and liquid slug during air mixing by photographing the motion of plastic balls in the pipe with a video camera. In fact, the behavior of small acrylic balls 9.5 mm in diameter and 1.15 in specific gravity in the pipe was captured with the video camera and was analyzed.

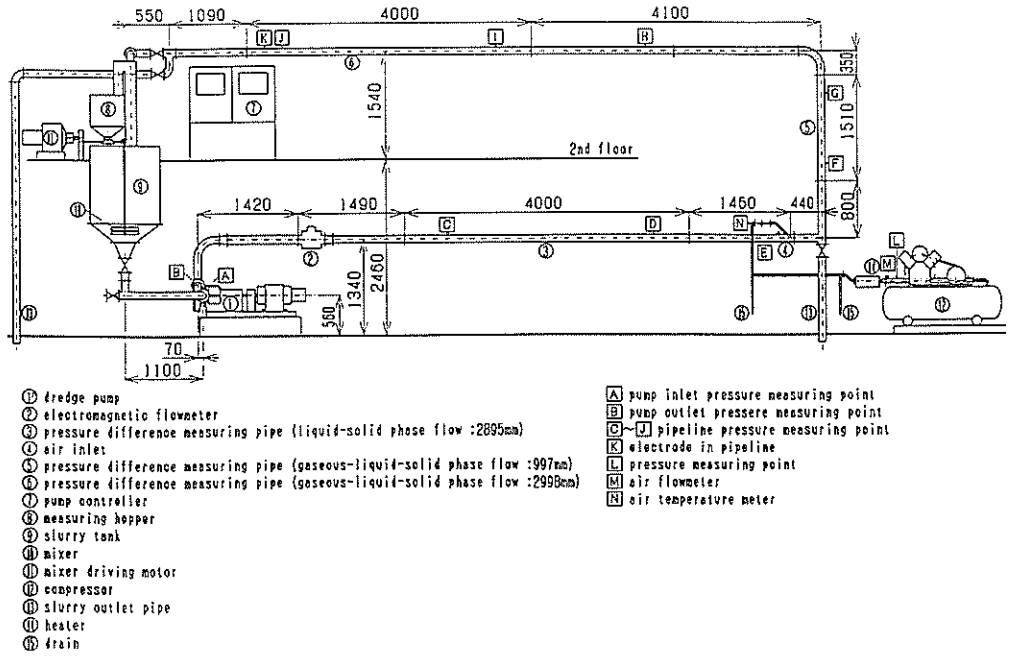

Fig. 1 Schematic diagram of flowing test loop

2.2 Outline of the Air Pressured Transport Equipment in the Field and the Measuring Method

2.2.1 Field Measurement in Mie

Figure 2 shows the outline of the air pressured transport system used in Mie. This was used for dredging works performed in Inabe Town, Inabe County, Mie Prefecture for transporting waste slag to a dumping place 1300 m away after cutting stone material.

Whole of the air pressured transport equipment including the dredging machine

was set on a pontoon; mud collected by a marsh travelling vehicle is placed into a hopper by backhoe. A screw pump is connected to the bottom of the hopper; and muddy slurry pulled out by the screw pump is slightly pressured by a centrifugal pump and sent to the air blowing hole. This point is noted as P_1 in the figure.

The transport pipe is gradually raised in increments of approximate up to the 600 m point. However, the length of sediment slurry phase in the pipe is much smaller than that of the gaseous phase, so that pressure loss due to this elevation can be almost ignored.

Distance from air blowing hole to pipe outlet is 1,300 m and pressure sensors are installed at the intervals of 300 m from P_1~P_5 as shown in **Fig. 2**. **Table 1** shows the principal specifications for the air pressured transport equipment.

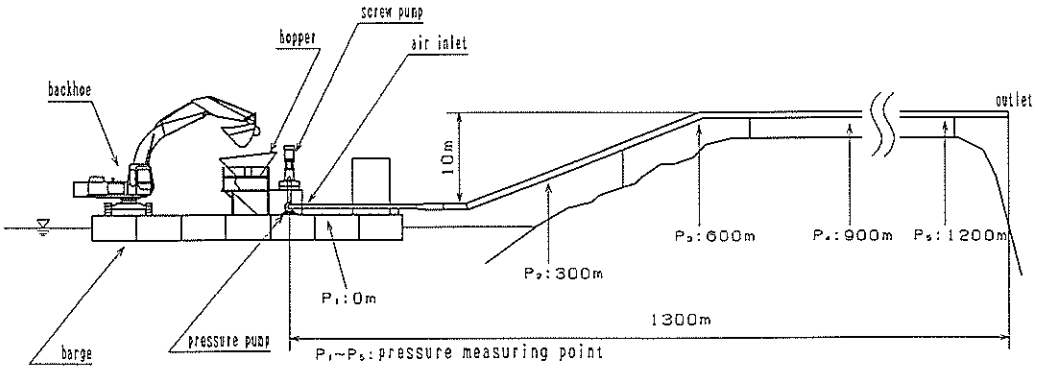

Fig. 2 Schematic diagram of field plant pipeline in MIE

Table 1 Specification of field plant

	Mie: air pressure plant (100m³/h)			Kumamoto: air pressure plant (300m³/h)		
1)material	mud (80% over raito of moisture content)			mud (80% over raito of moisture content)		
2)pressure capacity	100(m³/h)×1300(m) (nominal)			150(m³/h)×1000(m)×2 (nominal)		
3)transportable maximum diameter	80(mm)			120(mm)		
4)horsepower of dynamo / electric power supply	electric power supply: AC220(V) 60(Hz) 3φ 200(kVA)			main dynamo: 1030(PS)×1, 900(PS)×2 auxiliary dynamo: 240(PS)×1, 15.8(PS)×1 compressor: 203(PS)×4×2set		
5)diameter of pipe	350A			300A		
6)backhoe	1.4(m³)			2.0(m³)×2		
7)facilities	a)mud pump	·diameter of screw ·motor ·control system	300(mm) 45(kw) 8P VVVF	a)mud pump	·diameter of screw ·motor ·control system	370(mm) 90(kw) 8P VVVF
	b)inlet facility	·motor ·control system	22(kw) 8P VVVF	b)mixer	·type ·diameter of paddle ·motor	twin paddle φ700(mm) 18.5(kw) 4P
	c)compressor motor	·motor ·starting method	55(kw) 6P star-delta	c)compressor motor	·motor ·control system	132(kw) 6P VVVF
	d)hopper	·mesh ·dimension	300(mm)×400(mm) 2500(mm)×2500(mm)	d)vibration screen	·mesh ·motor	80(mm)×80(mm) 15(kw) 4P
	e)crasher	·motor	7.5(kw) 4P	e)sorter	·mesh	300(mm)×400(mm)
8)compressor	10(Nm³/min)×8			21.2(Nm³/min)×7(kgf/cm²) ×4×2set		

The measuring work was performed on 1st Dec. 1990. The items of **Table 2** were recorded continuously with pen-recorder. As the recording speed of the data of Mie was slower than the data of Kumamoto, it was at times difficult to catch the change of data clearly like that of Kumamoto.

Table 3 shows the list of work achievements such as the mean air discharge for each measuring case, and mean slurry discharge, etc. And the air discharge is calculated from the rated capacity of compressor; this is the same for the case of Kumamoto.

Table 2 Measuring item and measuring method

Mie		Kumamoto	
measuring items	measuring method	measuring items	measuring method
pressure(screw-pump) P_{sp}	pressure gage	pressure(screw-pump) P_{sp}	pressure gage
pressure(0m) P_1	pressure gage	pressure(0m) P_1	pressure gage
pressure(300m) P_2	pressure gage	pressure(150m) P_2	pressure gage
pressure(600m) P_3	pressure gage	pressure(330m) P_3	pressure gage
pressure(900m) P_4	pressure gage	density of slurry	γ -radiation density meter
pressure(1200m) P_5	pressure gage	flow rate of adding water	electromagnetic flowmeter
flow rate of slurry	electromagnetic flowmeter	flow rate of slurry	electromagnetic flowmeter
power of inlet motor	ampere meter	revolution of screw	tachometer
power of screw motor	ampere meter	revolution of pressure pump	tachometer
ampere of pump motor	ampere meter	ampere of screw motor	ampere meter
revolution of inlet	pulse detector	ampere of pressure pump motor	ampere meter
revolution of screw	pulse detector	pressure(air pipeline) P_{air}	pressure gage
density of slurry	analysis after sampling		

Table 3 List of average measuring field data

	MIE		KUMAMOTO	
common value	mean particle size (50%)	d_{50}=0.008 (mm)	mean particle size (50%)	d_{50}=0.035 (mm)
	mean slurry ture specific gravity	γ_s =2.65	mean slurry ture specific gravity	γ_s =2.684
	mean slurry density	ρ_m =1440 (kg/m³)	mean slurry density	ρ_m =1600 (kg/m³)
	rated flow of one compressor	10 (Nm³/min)	rated flow of one compressor	21.2 (Nm³ /min)
	diameter of discharge pipeline	350A (=339.8(mm))	diameter of discharge pipeline	300A (=304.7(mm))
	length of discharge pipeline	1300 (m)	length of discharge pipeline	357.8 (m)
	pressure measuring point	0, 300, 600, 900, 1200 (m)	pressure measuring point	0, 150, 330 (m)
case 1	the number of compressor	6 (=60 (Nm³/min))	the number of compressor	3 (=63.6 (Nm³/min))
	mean slurry flow rate	49.68 (m³/h)	mean slurry flow rate	247.5 (m³/h)
	mean slurry velocity	0.152 (m/s)	mean slurry velocity	0.947 (m/s)
	mean slurry density	1463 (kg/m³)	mean slurry density	1596 (kg/m³)
case 2	the number of compressor	5 (=50 (Nm³/min))	the number of compressor	2 (=42.4 (Nm³/min))
	mean slurry flow rate	57.53 (m³/h)	mean slurry flow rate	220.0 (m³/h)
	mean slurry velocity	0.176 (m/s)	mean slurry velocity	0.842 (m/s)
	mean slurry density	1446 (kg/m³)	mean slurry density	1619 (kg/m³)
case 3	the number of compressor	4 (=40 (Nm³/min))		
	mean slurry flow rate	33.99 (m³/h)		
	mean slurry velocity	0.104 (m/s)		
	mean slurry density	1440 (kg/m³)		
case 4	the number of compressor	8 (=80 (Nm³/min))		
	mean slurry flow rate	30.07 (m³/h)		
	mean slurry velocity	0.092 (m/s)		
	mean slurry density	1420 (kg/m³)		

2.2.2 Field Measurement in Kumamoto

In Kumamoto, sediment is dredged from a mooring basin and seaway and is shipped by sealed barges and then discharged to a reclamation area from the barge by an air pressured transport plant[10]. This plant is the pipeline transport system of high density mud with air mixture called 4th Construction Bureau Type, the same as that of Mie. In this paper, the various continuous data gathered by the construction work were compared with the result of the laboratory experiment and the data of Mie.

Figure 3 shows the situation of overall piping and pressure sensors installed. Length from air blowing portion to the pipe outlet is 358 m, and pressure sensors are installed on the pipe at 4 positions of P_{sp}, P_1, P_2 and P_3.

Supply of sediment to the air pressured transport equipment is performed by using a backhoe from the barge berthed to the pontoon exclusively for the air pressured transport equipment. The same as the case of Mie, sediment supplied to the hopper is pushed out by the screw from the bottom of hopper to pipeline.

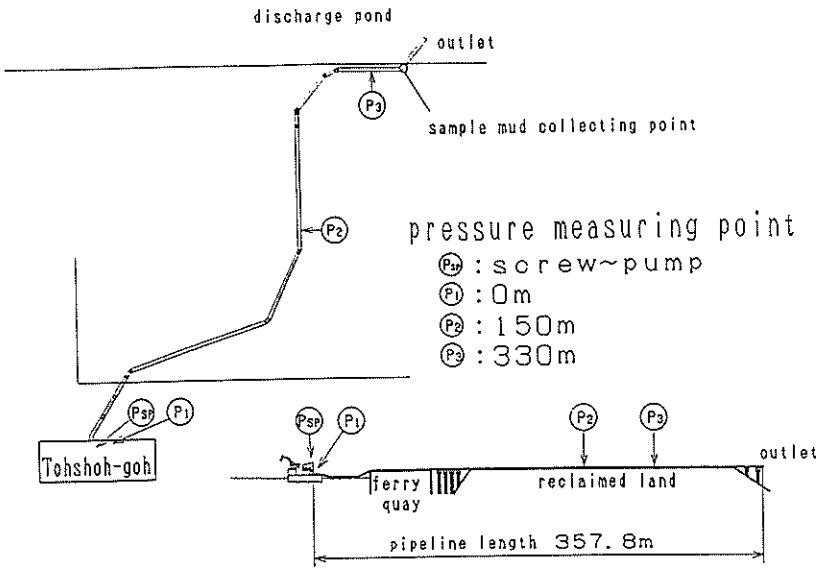

Fig. 3 Schematic diagram of field plant pipeline in KUMAMOTO

The muddy slurry pressured by a centrifugal pump meets air blown to the pipeline at point P_1. P_{sp} in the Figure means the pressure of slurry at the inlet of pressuring pump.

Figure 4 shows in detail the portion downstream of the air blowing portion on the pontoon for the plant. A γ-radiation densitometer and an electromagnetic flowmeter are set between a pressuring sand pump and the air blowing portion. Therefore, the values measured at this portion express the density and discharge of slurry alone containing no air.

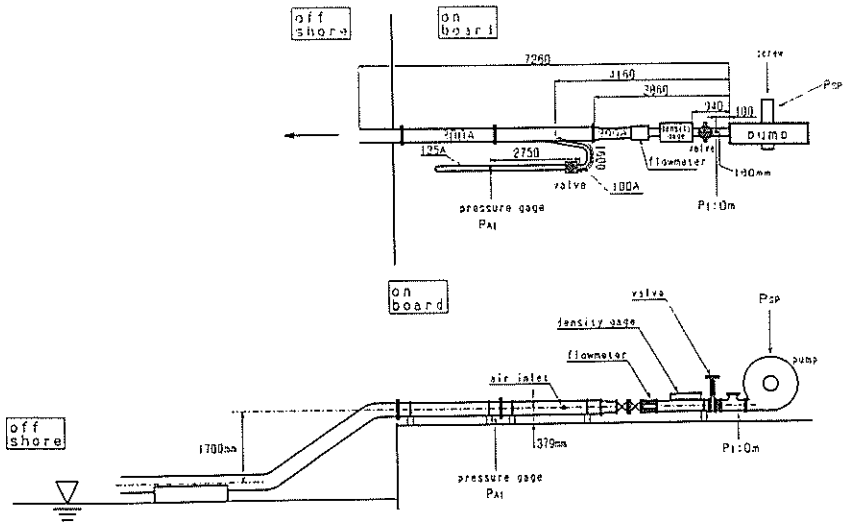

Fig. 4 Schematic diagram of field plant pipeline in KUMAMOTO

Pipe diameter downstream of the air blowing portion is 304 mm, and this pipe is connected to an air supply pipe 100 mm in diameter. In the figure, P_a is an air pressure sensor for blowing air immediately before meeting slurry. **Table 1** shows the main specifications of the plant and **Table 2** shows the measuring items and methods. The measuring work was performed under the working conditions as shown in **Table 3** on 4th Sept. 1991.

2.3 Sediment Used in Laboratory and Field Experiment

Figure 5 shows the particle size accumulation curve for muddy slurry used in Mie, and its 50% mean particle size is 0.008 mm and true specific gravity of particles is 2.65. Also as understandable from the grain size distribution in **Fig. 6**, the 50% mean grain size of Kumamoto is 0.035 mm, which is larger than that of Mie, and the true specific gravity of particles is 2.684.

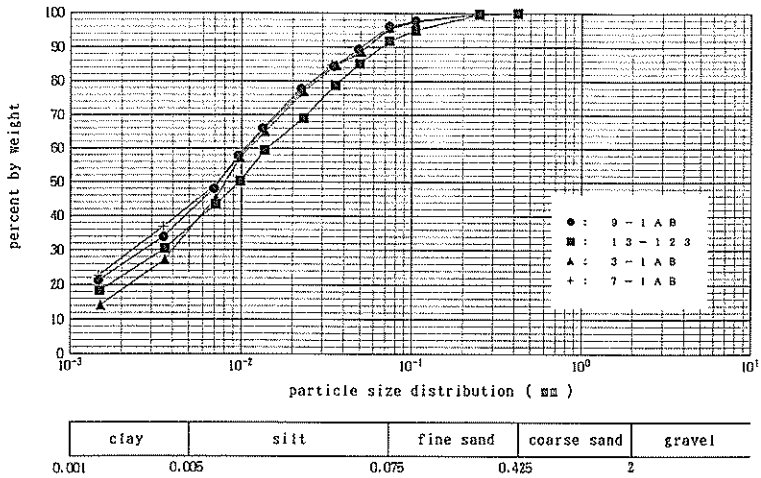

Fig. 5 Particle size accumulation curve in MIE

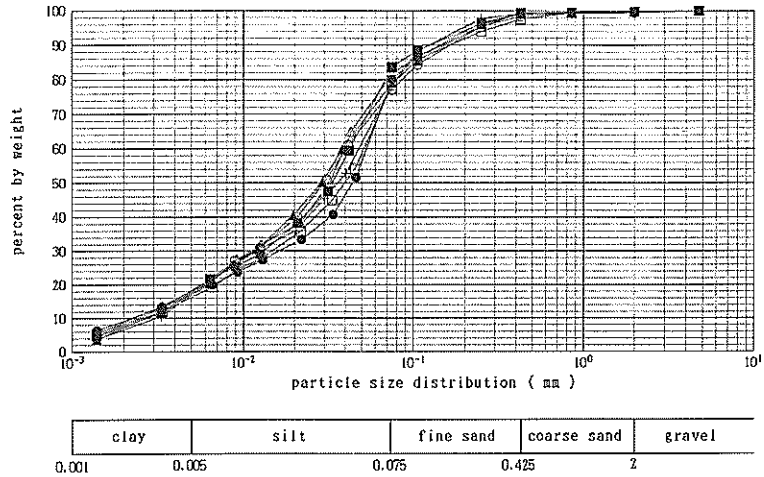

Fig. 6 Particle size accumulation curve in KUMAMOTO

3. Fluidity Characteristic of Solid-Liquid Slurry

3.1 Characteristics of Pressure Gradient of Muddy Slurry in Pipe

Figure 7 shows the pressure gradient when fresh water and mud (specific gravity is 1202 kgf/m³) flowed through an acrylic pipe used in the measuring section in laboratory experiment; it is indicated by the pressure loss per unit length relative to velocity.

By comparing the flow of fresh water and muddy slurry, it can be said that in the case of fresh water, the whole range of this experiment is a turbulent flow zone but in the case of muddy slurry, the laminar flow portion continues up to a considerable velocity. Because of this, it is characteristic in that the increasing tendency in pressure loss relative to the muddy slurry at the laminar flow portion is very flat compared to the fresh water. Also in **Fig. 7**, an apparent transition from the laminar flow to the turbulent flow zone can be recognized.

Therefore, in order to find the fluidity characteristics when air is mixed during such slurry flowing, it is necessary to arrange the flow pattern shown in **Fig. 8** and to estimate the fluidity characteristics of muddy slurry alone.

Here, the pressure loss during muddy slurry flowing will be reviewed by the method explained below including the transition region from laminar flow to turbulent flow.

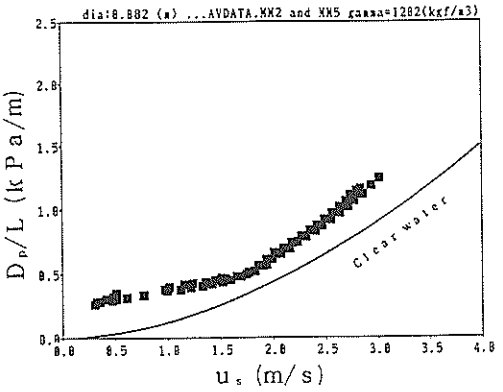

Fig. 7 Velocity u_s and pressure loss D_p/L for clear water and non-Newtonian slurry

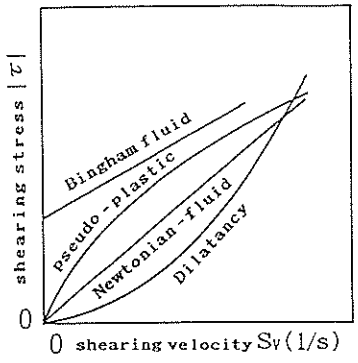

Fig. 8 Classification of fluid flow characteristic

3.2 Rheology Parameters for Power Law Model

Power law fluid is characteristic in that the shear stress is not linearly proportional to the velocity gradient. That is, the flow curve is expressed by exponents as shown below, it is called the fluid of exponent or power-law fluid. Also, if the exponent n is smaller than 1, then the fluid is called the psuedo-plastic fluid. (Refer to **Fig. 8**). The shearing stress at discretional point in pipe can be expressed by

$$\tau = K \cdot \left(-\frac{du}{dr} \right)^n \tag{1}$$

where, τ is shear stress, u is velocity and r is a distance from the center of pipe to the outside. From the velocity gradient of **Eq. 1**, it can be integrated under the condition that the fluid does not slip on pipe wall, and the velocity distribution in pipe can be

expressed by

$$u = \left(\frac{n \cdot r_o}{n+1}\right) \cdot \left(\frac{\tau_0}{K}\right)^{\frac{1}{n}} \cdot \left\{1 - \left(\frac{r}{r_o}\right)^{\frac{n+1}{n}}\right\} \tag{2}$$

where, τ_0 shows the shear stress at pipe wall r_0.

Now, if the mean velocity in pipe is u_s, then a relational expression using the mean velocity can be obtained by integrating the **Eq. 1** again. That is,

$$\tau_0 = K \cdot \left(\frac{3n+1}{4n}\right)^n \cdot \left(\frac{8u_s}{D}\right)^n \tag{3}$$

$(8u_s/D)$ in **Eq. 3** is called the shear rate or shear velocity.

If the shear stress τ_0 on wall surface and shear velocity determined from the flow data in pipe are plotted on logarithmic coordinates, and the results are almost a straight line in laminar flow portion, then

$$\tau_0 = K' \cdot \left(\frac{8u_s}{D}\right)^{n'} \tag{4}$$

where, u_s : Velocity of slurry

D : Pipe diameter

In the above equation, K' and n' are determined. **Figure 9** shows the results of finding shear stress from experimental data which are plotted together with shear velocity on a log-log graph. In this figure, the lateral coordinates S_v means the shear velocity $(8u_s/D)$.

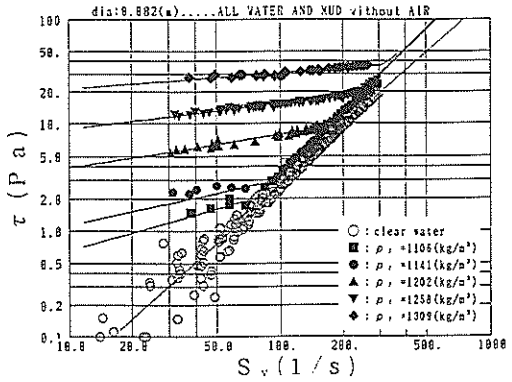

Fig. 9 Shearing velocity S_v and shearing stres τ for MIE's slurry (ρ_f = 1202 kg/m³)

That is, from **Eqs. 3** and **4**, the rheology parameters for the power law model of pseudo-plastic fluid can be determined as follows:

$$n = n'$$

$$K = K' \cdot \left(\frac{4n}{3n+1}\right)^n \tag{5}$$

By plotting n (rheology index) obtained above and K (consistency coefficient) relative to the slurry density, it can be known as shown in **Figs. 10** and **11** that the rheology parameters have a strong correlation with the slurry density. From these tendencies, the value for the mud in the field of Mie is estimated in this paper. Namely the values for the density of mud in the field of Mie is 1440 kg/m³; thus the following can be obtained:

$n = 0.072$

$K = 218.0$ (Pa · s^n)

Table 4 summarizes the parameters derived from the laboratory experiment and the result of the estimation.

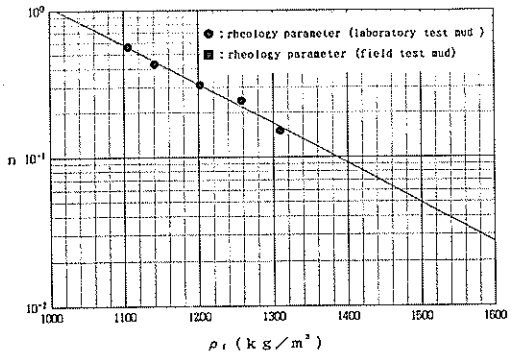

Fig. 10 Slurry density ρ_f and rheology index number n

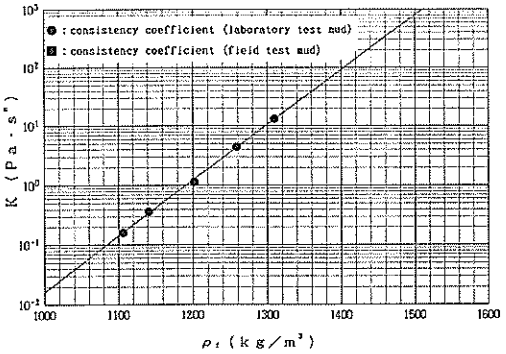

Fig. 11 Slurry density ρ_f and consistency coefficient K

Table 4 Physical properties of mud slurry

	Mie			Kumamoto		
	ρ_f (kg/m³)	n	K (Pa·s^n)	ρ_f (kg/m³)	μ_B (Pa·s)	τ_y (Pa)
laboratory experiment	1106	0.56	0.1646	1202	0.00853	2.612
	1141	0.43	0.3753	1273	0.014	6.00
	1202	0.31	1.660	1388	0.03054	23.38
	1258	0.24	4.485			
	1309	0.15	13.27			
field experiment	1440	0.072	218.0	1600	0.125	260.0

3.3 Rheology Parameters for Bingham Fluid

Figure 12 shows the results of experiments on the mud taken at Kumamoto and transported; the experiments were conducted by using laboratory fluidity experiment equipment. As a result of trial and error, it was clarified that the fluidity model should be rather handled as a Bingham fluid model instead of considering a power law model in view of the method of change in laminar flow portion and the situation of transition

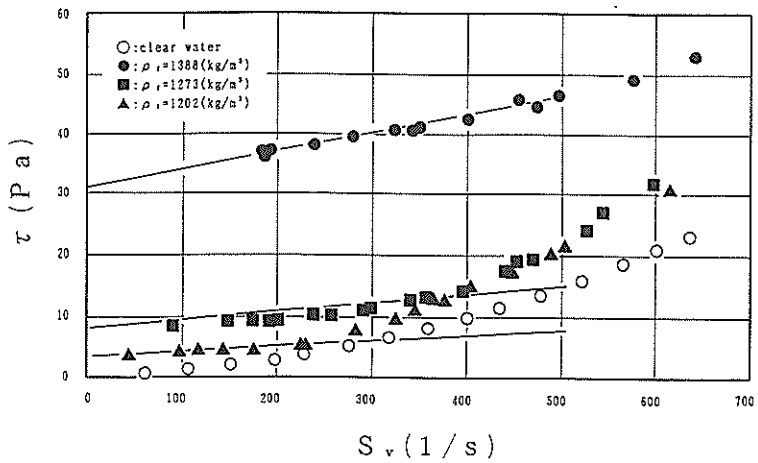

Fig. 12 Shearing velocity ρ_f and shearing stress τ for KUMAMOTO's slurry

to turbulent flow, being different from the case of the mud in Mie.

In this case, the fluidity parameters are determined as follows:

In the Bingham fluid model, if the shear stress is τ at the point with a distance r from the center of pipe and the yield stress is τ_y, than the shear stress for velocity gradient can be expressed as follows:

$$\tau - \tau_y = \mu_B \cdot \left(-\frac{du}{dr}\right) \qquad \tau \geqq \tau_y \tag{6}$$

$$\frac{du}{dr} = 0 \qquad \tau < \tau_y \tag{7}$$

As understandable from **Eqs. 6** and **7**, the velocity becomes constant near the center of pipe where $\tau < \tau_y$ since there is no shearing stress, and the velocity distribution will have a form of plug at the center of pipe.

Now, if the radius from the center of pipe for plug portion is r_y and the radius of pipe is r_0, then

$$a = \frac{\tau_y}{\tau_o} = \frac{r_y}{r_o} \tag{8}$$

This "a" is called the specific plug radius. By using the specific plug radius a and **Eqs. 6, 7** and **8**, the velocity u at a given point in the pipe can be expressed by

$$u = \frac{\tau_o \cdot r_o}{2 \cdot \mu_B} \cdot \left\{ 1 - 2a + 2a \cdot \left(\frac{r}{r_o}\right) - \left(\frac{r}{r_o}\right)^2 \right\} \tag{9}$$

Now, if the mean velocity in pipe is u_s, then the following relation can be obtained between shear rate S_v and shear stress τ_0, at pipe wall:

$$S_v = \frac{8 \cdot u_s}{D} = \frac{\tau_o}{\mu_B} \cdot \left(1 - \frac{4}{3}a + \frac{a^4}{3}\right) \tag{10}$$

Since $a^4 \fallingdotseq 0$ can be deemed in the region where S_v is large, the following relation is obtained:

$$\tau_0 \fallingdotseq \mu_B \cdot S_v + \frac{4}{3}\tau_y \tag{11}$$

That is, if shear stress τ_0 at wall surface obtained from experiment data is plotted relative to shear rate S_v and this becomes a relation close to the **Eq. 11**, then the muddy slurry being considered can be handled as a Bingham fluid model. The fluid model explained above was determined by considering the points stated here.

By applying **Eq. 11** to the laminar flow portion of these data, the yield stress τ_y and the Bingham viscosity coefficient μ_B can be determined. There were four kinds of muddy slurry density in the laboratory fluidity experiment for Kumamoto mud. As shown in **Figs. 13** and **14** τ_y, μ_B changed for each density. From this tendency, the following values were obtained for the density of 1600 kg/m³ of the mud in the field of Kumamoto:

$\tau_y = 260.0$ (Pa)

$\mu_B = 0.125$ (Pa · s)

Table 4 summarizes the relation between the density and τ_y, μ_B in the laboratory fluidity experiment and the values of τ_y and μ_B estimated for the mud in field. Of course, each correlational equation agrees with the mud used in Mie and Kumamoto, but it has no generality.

When determining the transport conditions while adjusting the density of mud in the field, the rheology parameters for a given value of slurry density can be determined by obtaining such a correlation by a certain method.

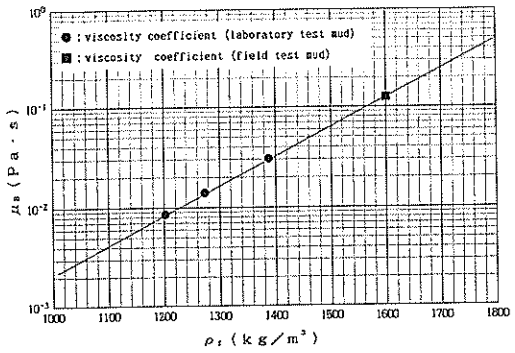

Fig. 13 Slurry density ρ_f and viscous coefficient μ_B

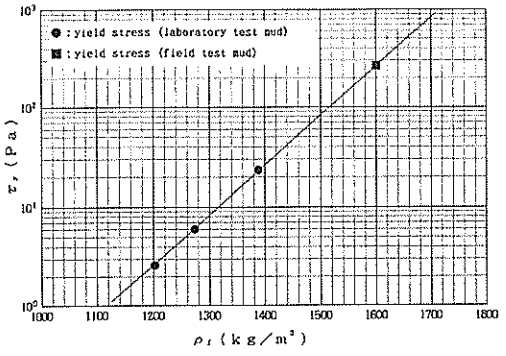

Fig. 14 Slurry density ρ_f and yield number τ_y

3.4 Method of Estimating Pressure Gradient in Pipe

The pressure loss per unit length of solid-liquid slurry during flow through pipe can be determined as follows:

$$D_p/L = \frac{4 \cdot f \cdot \rho_f \cdot u_s^2}{2 \cdot D} \tag{12}$$

where, f is Fanning's friction loss coefficient and ρ_f is the density of slurry.

The flow gradient in the case of fresh water is flown in the acrylic pipe which is used in the measuring point of this experiment is calculated by **Eq. 12**. The pipe

friction loss coefficient f_w is usually calculated by Blasius's equation etc. In this case, the experimental equation which agrees with the actual fresh water flowing data is decided as follows.

$$f_w = 0.048 \cdot {R_e}_l^{-0.2} \qquad (13)$$

$${R_e}_l = \frac{\rho_w \cdot D \cdot u_s}{\mu_w}$$

If μ_w is the coefficient of viscosity of fresh water:

This has a slightly different tendency from Blasius's equation and is extremely close to the equation by Knudsen and Katz[11].

The ways to determine the pipe friction loss coefficient for solid-liquid slurry are shown separately for power law fluid and Bingham fluid.

When Metzner-Reed's Reynolds number [12] is given by

$$R_{eMR} = \frac{\rho_f \cdot D^n \cdot u_s^{(2-n)}}{K} \cdot 8 \cdot \left(\frac{n}{6n+2}\right)^n \qquad (14)$$

then, the friction loss coefficient for the laminar flow portion can be obtained for the following value:

$$f = \frac{16}{R_{eMR}} \qquad (15)$$

That is, if a deformed Reynolds number adopting a rheology parameter as shown in **Eq. 14** is selected, then the friction loss coefficient can be obtained in the form of **Eq. 15** the same as ordinary Newtonian fluid with respect to the laminar flow portion.

Finding f from **Eq. 15** and computing the pressure loss is applicable for the laminar flow portion because the relation of **Eq. 3** was established for laminar flow. Expressed reversely, with respect to the portion deviated and shifted from the laminar flow to the turbulent flow, there will be no guarantee whether the rheology parameters determined in the laminar flow range are effective or not. However, here, the rheology parameters were used for uniform handling even at the transition point to turbulent flow and in the transition zone.

With respect to the transition from the laminar flow to turbulent flow, we graphically determined the transition point from experimental data and the critical Reynolds number reported by Masuyama et al., [13] indicated below.

$$R_{eMRC} = \frac{2240 \cdot (2n+1) \cdot (3n+2)}{(3n+1)^2} \qquad (16)$$

Then, we compared the critical Reynolds number R_{eMRC} and the transition point obtained from the graph of the experimental data. The result of comparison with the transition Reynolds number obtained from the experimental data and the critical Reynolds number of the **Eq. 16** is shown in **Fig. 15.** It can be said that both agree fairly well. These results were also compared to the critical Reynolds number determined from the friction loss coefficient at transition start point by Ryan and Johnson[14] indicated in **Eq. 17**; it is shown that **Eq. 17** shows the reverse tendency of **Eq. 16** particularly in the portion where the rheology index n is small.

$$R_{eMRC}=\frac{16\times 404}{\varnothing(n)}$$
$$\varnothing(n)=\frac{(3n+1)^2}{n}\cdot\left(\frac{1}{n+2}\right)^{\frac{n+2}{n+1}} \tag{17}$$

Here, the transition point from the laminar flow will be computed by using **Eq. 16.**

With respect to the turbulent portion deviated from the laminar flow, the friction loss coefficient is calculated by the following equation by considering the exponents in the empirical formula (13) related to the friction loss coefficient during water supplying obtained from experimental data:

$$f=f_c\cdot\left(\frac{R_{eMR}}{R_{eMRC}}\right)^{-0.2} \tag{18}$$

where, f_c is the value of **Eq. 15** substituting the critical Reynolds number determined from **Eq. 16.** That is, the friction loss coefficient at the turbulent portion takes f_c value at the critical Reynolds number and thereafter changes with the same exponent of the friction loss coefficient during water supplying.

The pipe friction loss coefficient f determined above was compared to the value derived from experimental data taken at the portion where the laminar flow portion and laminar flow transit to turbulent flow, and one example of this is shown in **Fig. 16.** Almost satisfactory results were obtained even in the transition zone to the turbulent flow. However, within the range where the Reynolds number increases further, f will naturally approach the line for fresh water; if the range with a much larger Reynolds number is considered, it will be necessary to newly review the function proposed by Kemblowski et al., [15].

In **Fig. 17**, the pressure loss per unit length for solid-liquid slurry calculated from the **Eq. 12** by using the pipe friction loss coefficient derived as stated above is compared to the experimental data. This figure shows all data of all experiment cases at once.

On the other hand, there are various equations for the indication of the Reynolds number for Bingham fluid model; Tomita's method will be adopted here.

Now, if the following conditions occur,

$$R_{eb}=\frac{\rho_f\cdot u_s\cdot D}{\mu_B} \tag{19}$$

$$\varnothing=1-\frac{4}{3}a+\frac{a^4}{3} \tag{20}$$

then Tomita's Reynolds number can be given by

$$R_{ebt}=R_{eb}\cdot\varnothing\cdot(1-a) \tag{21}$$

By using this Reynolds number, the pipe friction loss coefficient f for the laminar flow portion can be determined by the following deuations:

$$f_{bt}=\frac{16}{R_{ebt}} \tag{22}$$
$$f=f_{bt}\cdot(1-a) \tag{23}$$

For the turbulent flow zone, the following is obtained by using Karman-prandtl's equation:

$$\frac{1}{\sqrt{f_{bt}}} = 4 \cdot log\left\{R_{ebt} \cdot \sqrt{f_{bt}}\right\} - 0.4 \tag{24}$$

Conversion to the final pipe friction loss f is performed with **Eq. 23.**

Also in this paper, the transition from laminar flow to turbulent flow for Bingham fluid is not specially discussed, and the friction loss was calculated by using the larger value of the two friction loss coefficients described above. In consequence, this kind of method seems to agree fairly well with the situation of data transition obtained this time.

Figure 18 compares the pressure loss per unit length calculated from **Eq. 12** to the laboratory slurry transport data by using the pipe friction loss coefficient obtained as explained above. The results agree fairly well for both the laminar flow portion and turbulent flow portion. From this, the validity of handling the Kumamoto mud by Bingham fluid model can be understood. In general, it also seems appropriate to use the Bingham fluid model for the Kumamoto mud[16].

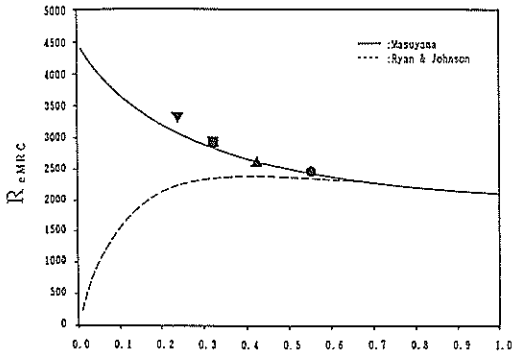

Fig. 15 Rheology index number n and critical Reynolds number R_{eMRC}

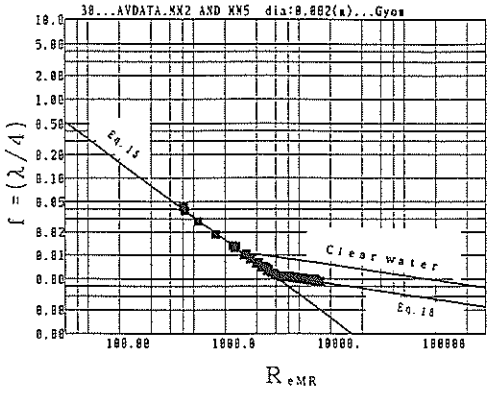

Fig. 16 Reynolds number R_{eMR} and friction factor f for MIE's slurry ρ_f = 1202 kg/m3

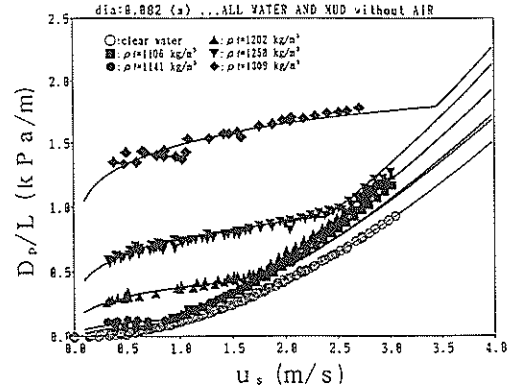

Fig. 17 Velocity u_s and pressure loss D_p/L for MIE's slurry

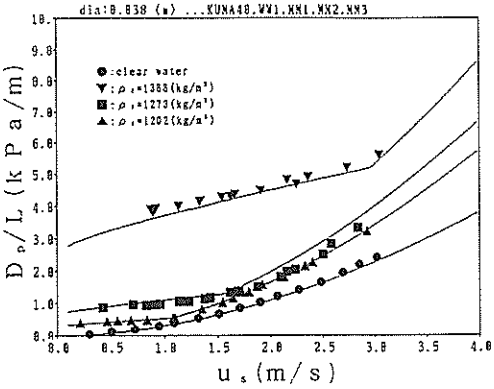

Fig. 18 Velocity u_s and pressure loss D_p/L for KUMAMOTO's slurry

4. Fluidity Characteristics of Slurry with Compressed Air in Horizontal Pipe (Laboratory Experiment)

4.1 Mean Void Ratio in Horizontal Pipe

Generally, a flow containing air and moving through a pipe dose not always have the same velocity for different phases, therefore, the proportion of gaseous phase at a certain part of the horizontal pipe, that is, void ratio α, normally has a different value from air discharge ratio X_v. Here, X_v is defined by

$$X_v = \frac{Q_a}{Q_a + Q_s} \tag{25}$$

Q_a is the amount of air; and the amount of air divided by the cross sectional area of pipe A, is called the apparent air velocity and given by

$$u_a = \frac{Q_a}{A} \tag{26}$$

In the same manner, Q_s is the discharge of liquid or solid-liquid slurry and its apparent velocity is expressed by

$$u_s = \frac{Q_s}{A} \tag{27}$$

Therefore, if X_v is expressed by respective apparent velocity,

$$X_v = \frac{u_a}{u_a + u_s} \tag{28}$$

Normally, the actual measurement of void ratio is an extremely difficult task, and thus few achievements on the estimate of void ratio obtained in the past are utilized in most cases. However, the void ratio is an important parameter for analyzing a flow containing air, and the error in estimating the void ratio will greatly affect the results.

Therefore, in this research, the average void ratio was measured by the method stated in the paragraph for experiment method, and the conventional void ratio estimating equation was corrected by using the average void ratio.

Inoue et al.,[17] made a dimensional analysis of the relative velocity ratio to each phase of gas and liquid and finally obtained the equation containing influences by density ratio and discharge ratio of each phase.

In the equation, the air discharge ratio X_v is introduced and then summarizing by void ratio α, the following formula is obtained:

$$\alpha = \frac{1}{1 + B_k \cdot \left(\frac{\rho_f}{\rho_a}\right)^{0.46} \cdot \left(\frac{1 - X_v}{X_v}\right)^{0.25} + \frac{1 - X_v}{X_v}} \tag{29}$$

Here, the influence of discharge ratio and density ratio upon the void ratio was made the same as in original equation and then B_k suited to this experiment was selected by comparing the **Eq. 29** to the data related to the measured void ratio and air discharge ratio at that time. Whereas B_k of the original equation is 0.025. Comparison of **Eq. 29** and measured data is shown in **Fig. 19** and **Fig. 20**. From both the figures it can be

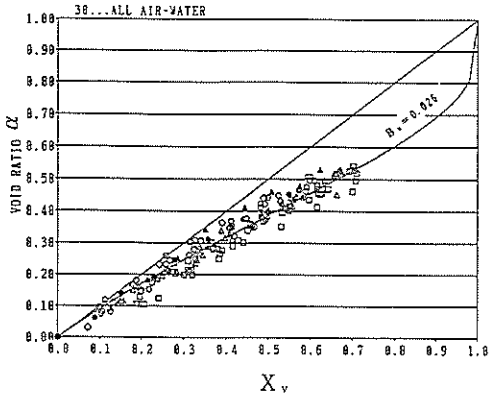

Fig. 19 Air flux ratio X_v and void rate α for air and clear water in trubulent flow

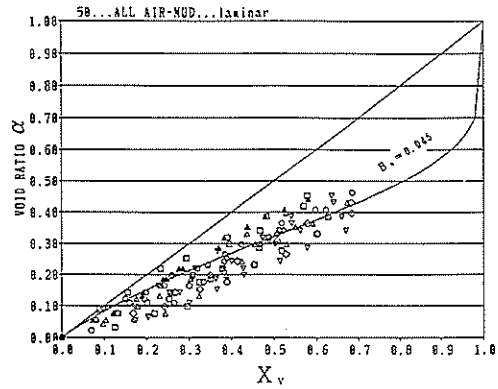

Fig. 20 Air flux ratio X_v and void rate α for air and slurry in laminar flow

known that considerably different values occur between the turbulent flow mainly comprising air and liquid and the muddy slurry in the laminar flow portion. In the turbulent flow, 0.026 close to the original equation of Inoue et al., occurs but the laminar flow has 0.045, thereby suggesting that the velocity distribution is considerably different.

Whereas the void ratio is obtained by the laboratory experiment where the air discharge ratio is rather small, in the air pressuring plant $\alpha \fallingdotseq X_v$ was considered in most portions where the air discharge ratio is considerably high.

4.2 Velocity at Each Portion Containing Air

A flow containing air in a horizontal pipe can be schematically indicated as shown in **Fig. 21**. Now, an axis moving on air slug is ξ axis and the continuity of surrounding liquid will be considered from this ξ axis [18], then

$$A \cdot \left(V_s - V_a\right) = A \cdot \left(1 - \alpha_r\right) \cdot \left(V_f - V_a\right) \tag{30}$$

by arranging the above,

$$V_f = \frac{V_s - \alpha_r \cdot V_a}{1 - \alpha_r} \tag{31}$$

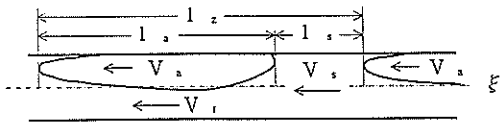

Fig. 21 Schematic diagram of air flow in horizontal pipe

can be obtained. Here, α_r is void ratio considered from the center of pipe in the radius direction. And if the void ratio in the longitudinal direction of pipe is α, then the following relation occurs:

$$\alpha = \frac{\alpha_r \cdot l_a}{l_z} \tag{32}$$

Amount of air Q_a supplied per unit time is

$$Q_a = \frac{A \cdot \alpha_r \cdot V_a \cdot l_a}{l_z} \tag{33}$$

Therefore, the absolute velocity V_a of air slug from **Eq. 32** and **Eq. 33** is given by

$$V_a = \frac{u_a}{\alpha} \tag{34}$$

On the other hand, the amount of liquid flowing in unit time, Q_s, is expressed by

$$Q_s = \frac{A \cdot V_s \cdot l_s}{l_z} + \frac{A \cdot \left(1 - \alpha_r\right) \cdot V_f \cdot l_a}{l_z} \tag{35}$$

From this equation, V_f and α_r can be removed by using **Eqs. 31** and **32**, then

$$Q_s = A \cdot V_s - A \cdot \alpha \cdot V_a \tag{36}$$

By substituting **Eq. 34** in the above equation, the absolute velocity V_s of liquid slug portion is as shown below independently from void ratio.

$$V_s = u_a + u_s \tag{37}$$

Velocity at each portion thus obtained was compared to the measured values obtained by photographing, with video camera, the colored plastic balls flowed with fresh water containing air and by analyzing their speed.

Figure 22 shows a plot of the absolute velocity of liquid in a liquid slug portion. It agrees fairly well with **Eq. 27**, but some data is significantly low. This seems to occur because the velocity of plastic balls held below air slug was also included during video camera analysis. For instance, **Fig. 23** shows the data only when the plastic balls are fully located below air slug, and the values are considerably smaller than V_s.

This velocity is theoretically given by **Eq. 31**. Calculating formula in the Figure is based on the assumption that the void ratio in pipe radius direction is equal to the void ratio in the longitudinal direction of pipe, and computation is made when u_s is maximum and minimum. **Equation 31** and experimental data agree fairly well.

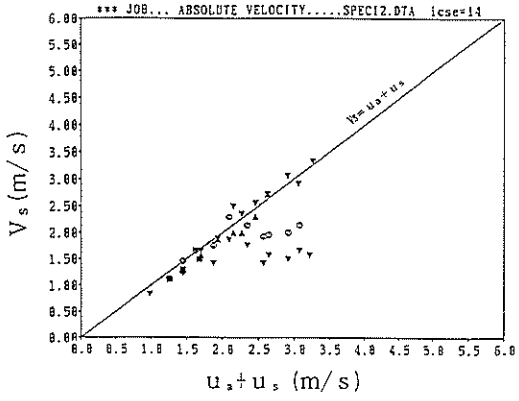

Fig. 22 Apparent velocity of air u_a + apparent velocity of slurry u_s and absolute velocity of liquid slug

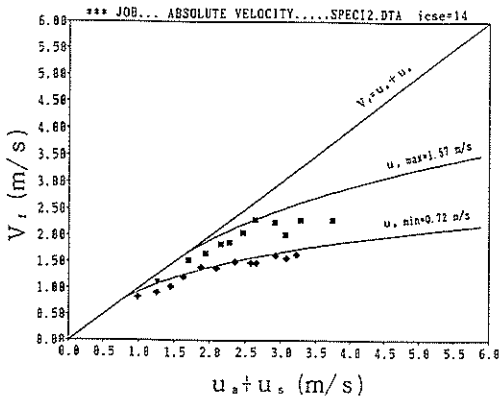

Fig. 22 Apparent velocity of air u_a + apparent velocity of slurry u_s and absolute velocity of liquid under air slug V_f

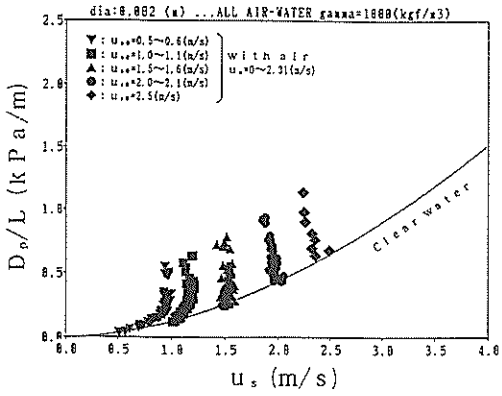

Fig. 24 Velocity u_s and pressure loss D_p/L for air injected clear water

Generally, the Nicklin's equation shown below is used for the air phase velocity.

$$V_a = 1.2 \cdot (u_a + u_s) \tag{38}$$

However, it is considered that $\alpha \fallingdotseq X_v$ in actual plant as mentioned before, it is subject to take $V_a \fallingdotseq V_s$ neglecting the slip between gas and slurry.

4.3 Pressure Loss in the Horizontal Pipe during Air Mixing

Figure 24 is a an example of showing a change in pressure loss when air is mixed while fresh water is flowing. In the case of fresh water, the pressure loss increases without exception when air is mixed.

Now, **Fig. 25 ~ Fig. 28** show the change by density in pressure loss per unit length when air is mixed in muddy slurry.

Data shown here includes the data where air volume is zero (u_{s0} in **Fig. 24 ~ Fig. 28**), and these data naturally agree with the pressure loss equation for Non-Newtonian

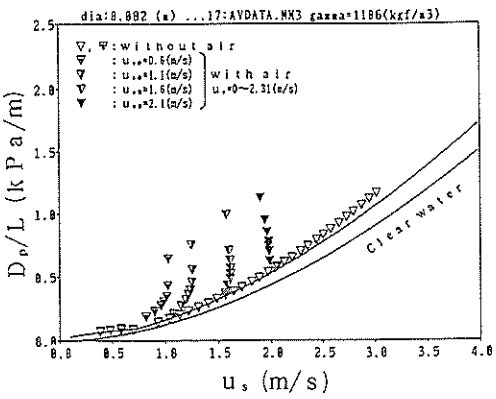

Fig. 25 Velocity u_s and pressure loss D_p/L for air injected MIE's slurry (ρ_f = 1106 kg/m³)

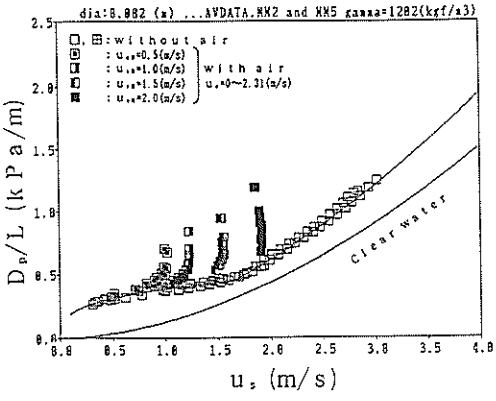

Fig. 26 Velocity u_s and pressure loss D_p/L for air injected MIE's slurry (ρ_f = 1202 kg/m³)

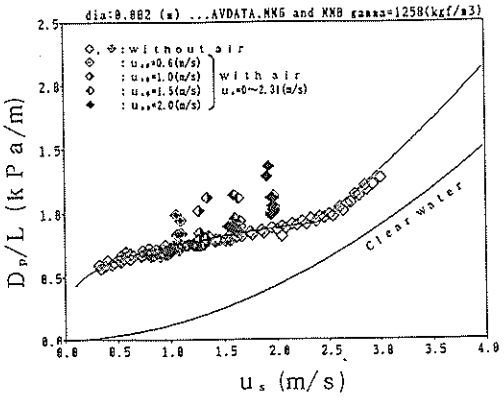

Fig. 27 Velocity u_s and pressure loss D_p/L for air injected MIE's slurry (ρ_f = 1258 kg/m³)

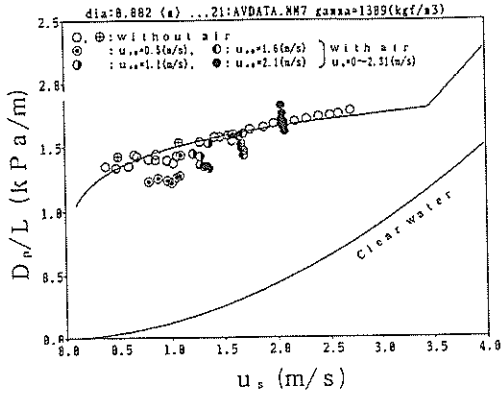

Fig. 28 Velocity u_s and pressure loss D_p/L for air injected MIE's slurry (ρ_f = 1309 kg/m³)

fluid obtained in Chapter 3. The slurry velocity at that time as standard state, the pressure loss is measured by gradually increasing air volume. Therefore, by considering mainly the pump, the resistance of the whole system fluctuates depending on the amount of mixed air. Particularly there is a vertical pipe portion almost 3 m long in this experiment equipment, and the air lift effect of this portion will increase when the slurry velocity is small[19].

In the pressure loss data in **Fig. 24** ~ **Fig. 28**, the slurry velocity fluctuates relative to the volume of blown air for the reason stated above.

Thus, the slurry velocity varies for a reason peculiar to the experiment equipment; therefore when reviewing the change in pressure loss during air mixing, in the strict sense of the word, it is necessary to make a comparison with the pressure loss value (for example, calculated value in Chapter 3) of muddy slurry containing no air relative to slurry velocity changed.

Under the prerequisite stated above, the effect of air mixing relative to the pressure loss per unit length of muddy slurry was checked, and the results were found

to be almost the same as the case of fresh water when the slurry density was low. However, if the density was high, the pressure loss sometimes decreased by mixing air, and this tendency was more significant as the density increased.

4.4 Horizontal Directional Separation Model and the Estimate of Pressure Loss

In a three-phase horizontal flow of gas, solid and liquid containing muddy slurry not easily settled and having a high air mixing ratio, it is more realistic to consider a model of which solid-liquid phase and gaseous phase are separated horizontal directionally.

That is, in **Fig. 21**, air slug should be considered well developed. At that time, how the velocity will be at each portion is calculated from the results of 4.2 and shown in **Fig. 29**. It can be known that value of V_f decreases as air volume increases, and air phase velocity V_a is not so great compared to liquid slug velocity V_s. Realistically thinking, flow loss of air phase is much smaller than liquid slug portion; the mean velocity of the whole can be considered as the liquid velocity V_s in liquid slug, and even the solid-liquid and gas are moving at V_s, no great loss occurs in the estimate of pressure loss.

That is, the pressure loss of the whole can be considered as a single loss divided by void ratio α of the portion being considered when the solid-liquid phase and gaseous phase are respectively flowing at the velocity V_s. This can be expressed by

$$D_{p2}/L = d_{p\_s} \cdot (1-\alpha) + d_{p\_a} \cdot \alpha \tag{39}$$

Here, d_{p_s} is the pressure loss per unit length when the solid-liquid phase is flowing at V_s and should be calculated by the method described in Chapter 3.

Also, d_{p_a} is the pressure loss per unit length when the air phase alone is flowing at velocity V_s. As the friction loss coefficient, it is calculated from the pipe friction loss coefficient during fresh water transport of **Eq. 13**. Also, as shown in **Eq. 37**, V_s is defined as the sum of apparent velocity u_a when the gaseous phase is assumed to flow alone and the velocity u_s when the solid-liquid phase is assumed to flow alone.

As stated in Par. 4.1, the void ratio is from the correlation between air discharge

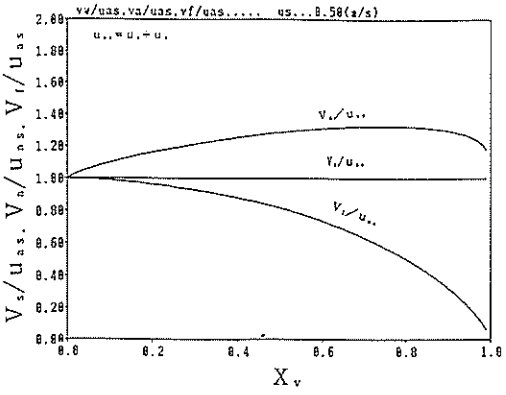

Fig. 29 Change of absolute velocity of liquid slug V_s, absolute velocity of air slug V_a and absolute velocity of liquid under air slug V_f for air flux ratio X_v

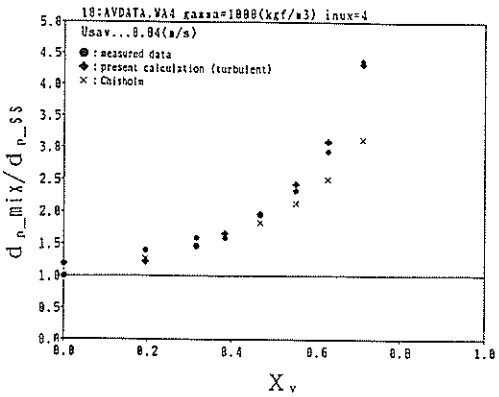

Fig. 30 Comparison of pressure loss ratio for clear water (Normal velocity u_{so} = 0.6 m/s)

ratio X_v and measured void ratio but the coefficient of the equation by Inoue et al., is slightly revised and used. Coefficient B_k is 0.045 for laminar flow and 0.026 for turbulent flow.

When the fluidity characteristics of solid-liquid slurry are apparent in the above method, the pressure gradient with mixed air gradually can be calculated. **Figs. 30~34** compares the change in pressure loss when air mixing ratio increases between the calculated values and measured values.

As stated above, individual solid-liquid slurry velocity, that is, u_s, of experimental data is not constant, the calculated values are determined in alignment with respective u_s. Also, the indication in the figure is not the pressure loss per unit length but a ratio to pressure loss per unit length of muddy slurry containing no air having u_s at that time.

It can be said that the **Eq. 39** shows that the calculated results are very close to the actual change from fresh water to high-density portion. Particularly, the changing tendency when the pressure loss ratio decreases below 1 at the high density portion is reflected relatively well, and the method used this time using the horizontal directional

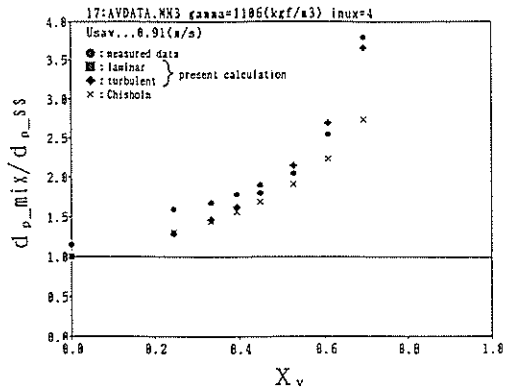

Fig. 31 Comparison of pressure loss ratio for MIE's slurry (Normal velocity u_{so} = 0.6 m/s, ρ_f = 1106 kg/m³)

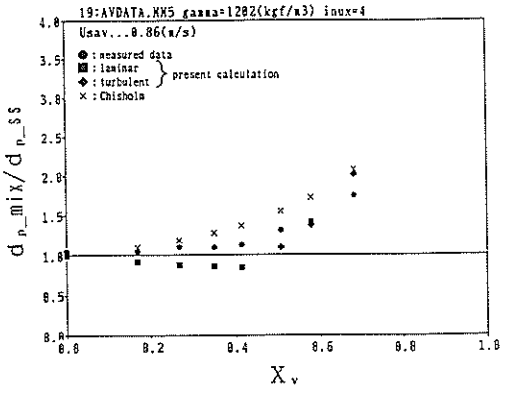

Fig. 32 Comparison of pressure loss ratio for MIE's slurry (Normal velocity u_{so} = 0.6 m/s, ρ_f = 1202 kg/m³)

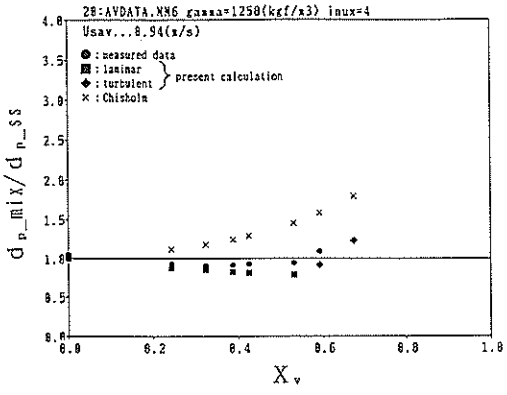

Fig. 33 Comparison of pressure loss ratio for MIE's slurry (Normal velocity u_{so} = 0.6 m/s, ρ_f = 1258 kg/m³)

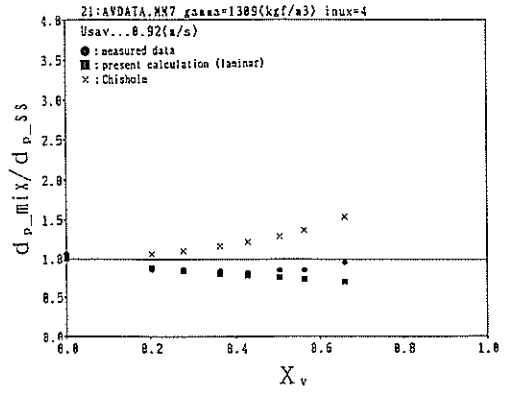

Fig. 34 Comparison of pressure loss ratio for MIE's slurry (Normal velocity u_{so} = 0.5 m/s, ρ_f = 1309 kg/m³)

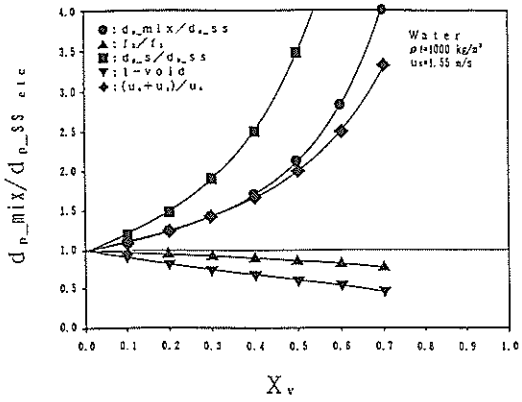

Fig. 35 Change of pressure loss ratio, etc., for air flux ratio X_v (clear water and air)

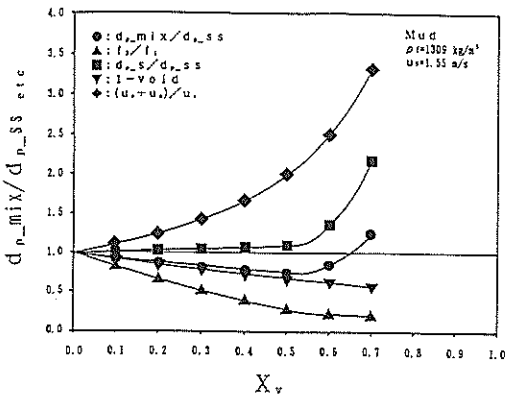

Fig. 36 Change of pressure loss ratio, etc., for air flux ratio X_v (MIE's slurry and air, ρ_f = 1309 kg/m³)

separation model seems to explain fairly well the fluidity characteristics at horizontal pipe of muddy slurry mixed with air.

That is, if air is mixed in fresh water or low-density slurry in the horizontal pipe, the mixing of air will result in the increase in pressure gradient, but it was found that flowing sometimes occurs at the resistance smaller than its own pressure gradient as the density becomes higher.

This mechanism is explained in **Fig. 35** and **Fig. 36**. These indicate how the various quantities such as velocity and friction loss coefficient change in response to mixed air volume compared to the case where no air is contained. When the fresh water and the solid-liquid slurry (the density is 1309 kg/m³) is flowing in pipe at the velocity of 1.55 m/s. Symbols used therein are listed below.

d_{p_mix}/d_{p_ss} : Ratio of air mixed slurry divided by void ratio relative to the pressure loss of slurry containing no air.

f_2/f_1 : Ratio of f_2 of air mixed slurry with the velocity increased relative to slurry of f_1 containing no air.

d_{p_s}/d_{p_ss} : Ratio of pressure loss of air mixed slurry with the velocity increased relative to pressure loss of slurry containing no air.

1-void : Proportion of dividing of pressure loss due to air mixture.

$(u_s + u_a)/u_s$: Increase in slurry velocity of the portion containing air due to air mixing.

Basically, when air is mixed, the velocity increases at each portion of gaseous phase and solid-liquid phase (refer to $(u_s + u_a)/u_s$). On the other hand, Reynolds number increases so that the friction loss coefficient reduction as indicated by f_2/f_1. Proportion of this decrease is small for fresh water because it is mostly in the turbulent zone. In consequence, pressure loss due to liquid slug as a result of the increased velocity bacomes very large (d_{p_s}/d_{p_ss}), and this means that the pressure loss is not sufficient for canceling by the decrease (can be considered as (1 – void ratio)) in the proportion of contact to the wall of liquid slug due to air mixing. In consequence, as seen in (d_{p_mix}/d_{p_ss}), the pressure loss of air mixed slurry becomes considerably high compared to the case where no air contained (d_{p_ss}).

On the other hand, in the case of high density slurry, the decrease in friction loss

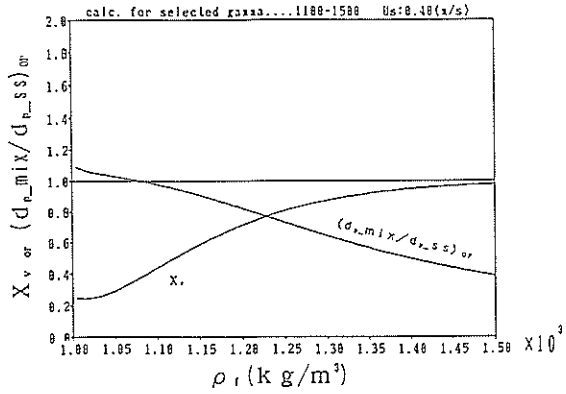

Fig. 37 Changes of air flux ratio X_v and pressure loss ratio d_{p_mix}/d_{p_ss} in optimum driving point for slurry density ρ_f

coefficient in this range is large since the laminar flow portion is much, and the pressure loss due to liquid slug as a result of the increased velocity will not be so large (refer to **Fig. 36**, (d_{p_s}/d_{p_ss})). Therefore, even though the decrease in the proportion of contact to wall surface of liquid slug due to air mixing is the same as the case of fresh water, it is possible that the pressure loss of air mixed slurry becomes smaller than the case where no air is contained.

This decreasing tendency, as understandable from the change in f_2/f_1 of **Fig. 36**, continues to the point where the range of solid-liquid velocity with mixed air is deviated from the laminar flow. That is, the point where the Reynolds number reaches the critical Reynolds number is the point where pressure loss ratio is the lowest. Thereafter, the pressure loss begins to increase again.

Above contents are very useful when reviewing actual transport condition of air mixed muddy slurry. For instance, in the case of transporting a certain amount of solid-liquid slurry, it becomes possible to review the optimum conditions on air blowing amount and the density adjustment of solid-liquid slurry. That is, we should be able to obtain the optimum operating point by adjusting the air volume in such a manner that, after mixing air in slurry in a certain state, the air volume is adjusted until the velocity increased by air mixing comes to the critical point. **Figure 37** shows the results of calculations for finding the optimum air blowing point of flowing slurry at the velocity of 0.4 m/s (no air contained) in horizontal pipe relative to the slurry density.

For instance, if the density is adjusted for making the specific gravity of 1.3 for slurry, then the air mixing ratio at the optimum operating condition will be about 85%; at that time, the pressure loss per unit length will become about 60% of that when slurry flows alone.

5. Flow of Muddy Slurry with Mixed Air in Actual Plant

5.1 Pressure Change during the Flow of Muddy Slurry with Mixed Air

Figure 38 shows an example of continuous recording of the slurry discharge and pressure at each point in pipe during the actual operation in Mie. Values for pipe pressure were obtained at 5 points P_1~P_5 at the same time as shown in **Fig. 2**, and the data with the highest pressure corresponds to P_1 and the lowest pressure to P_5.

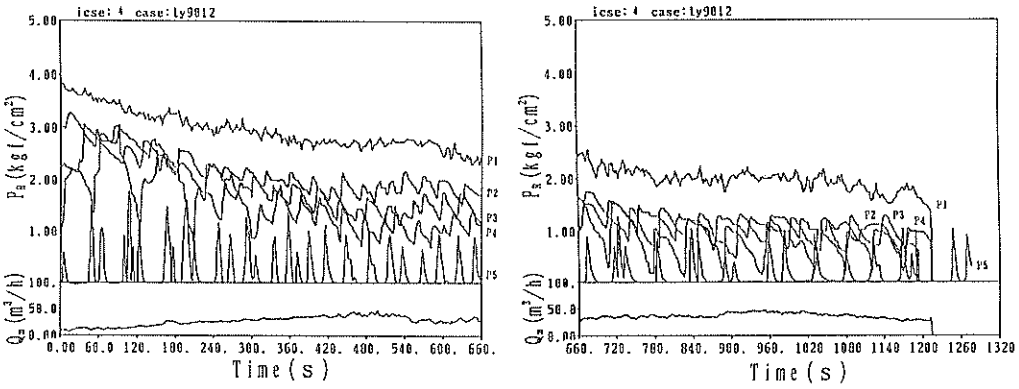

Fig. 38 Continuous data of field in MIE

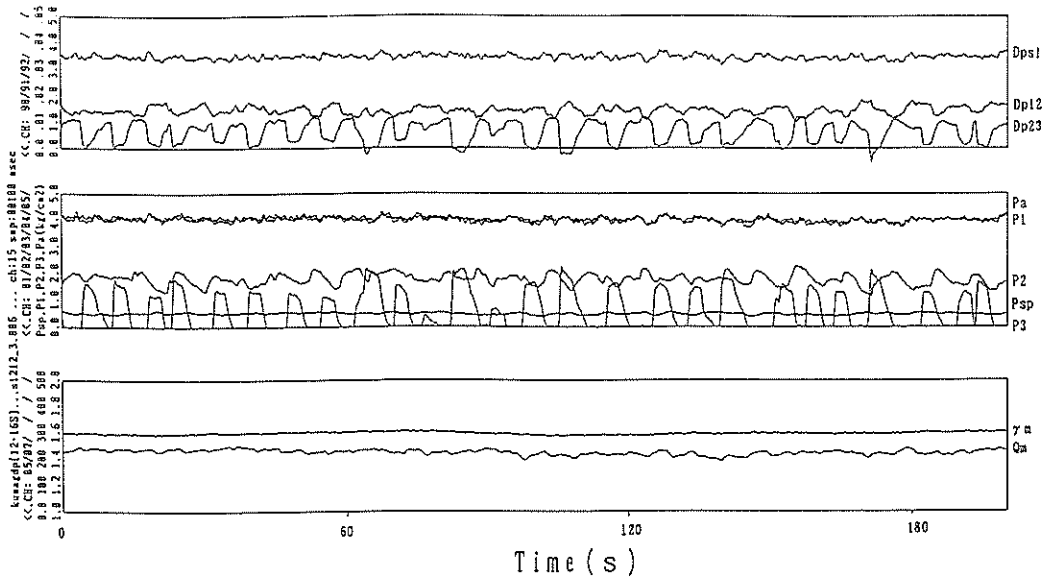

Fig. 39 Continuous data of field in KUMAMOTO

As a general tendency, wave fluctuation in pipe inner pressure becomes significant as slurry moves downstream, and the way of formation of so-called slug flow can be understood; that is, the solid-liquid slurry portion and air phase are gradually separated in pipeline (flow) direction.

Particularly, time of lowering of pressure at atmospheric pressure is long at P_5 and this means that there is no slurry occupying the whole surface of pipe from the pressure sensor P_5 to pipe outlet.

With the example of Kumamoto data shown in **Fig. 39** the pressure measuring points are not many but the same change appears as phenomenon.

This pressure changes and the width of change is shown in the histograms of **Figs. 40** and **41** in an easily understandable manner. According to Mie data, each pressure is fluctuating in the width of about 0.5 kgf/cm². Also, P_1~P_5 are the sensors respectively placed at the intervals of 300 m, so that the pressure loss per unit length at each point can

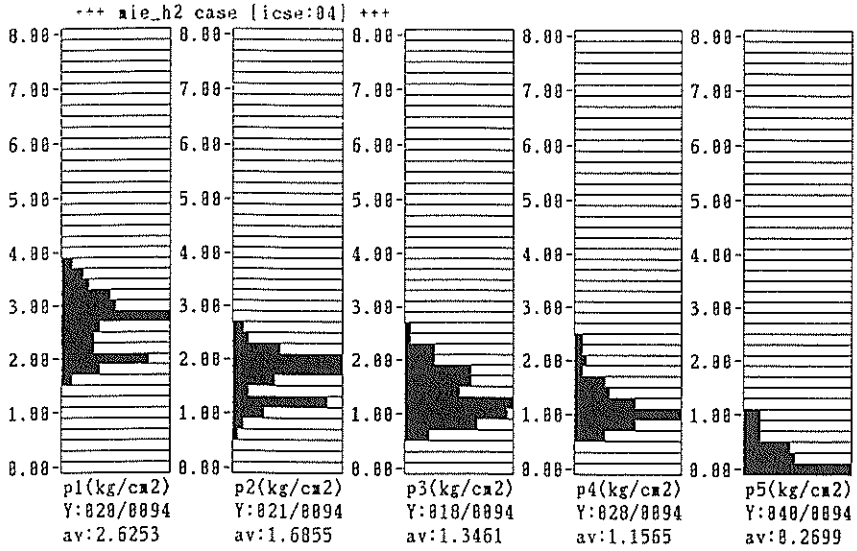

Fig. 40 Histogram of pressure data in MIE

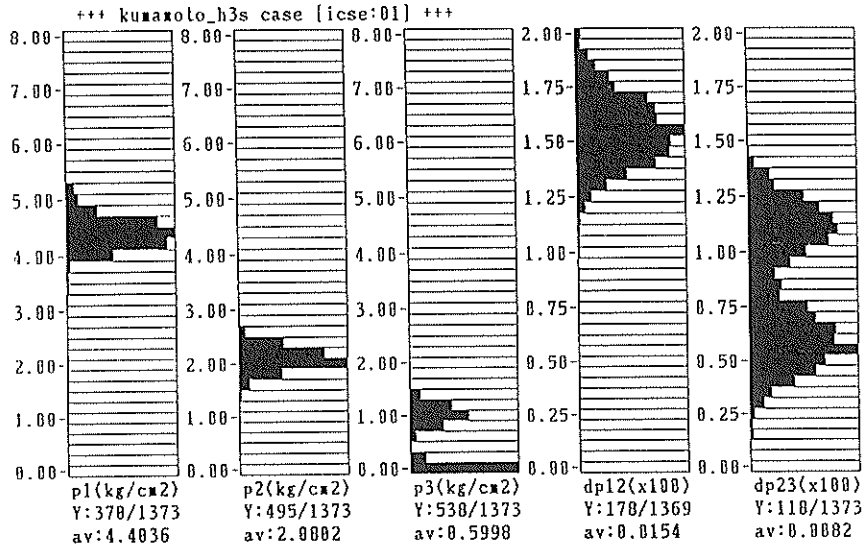

Fig. 41 Histogram of pressure data in KUMAMOTO

be compared with each other by checking the pressure loss between two adjacent points. From this, it can be known that the pressure loss at P_1~P_2 portion is greater than that after P_2.

The same tendency can be seen even for Kumamoto data. In this case, the distances among the pressure sensors P_1, P_2 and P_3 are all different, so that the histogram is prepared even for the pressure loss per unit length. It is apparent that the pressure loss per unit length is considerably different between P_1~P_2 and P_2~P_3. Also, there are two peaks in differential pressure between P_2 and P_3 probably because two states of presence and absence of the muddy slurry between the pressure sensor P_3 and pipe outlet are repeated.

5.2 Situation of the Separation of Slurry Phase and Air Phase

Being different from **Fig. 21**, the flow of air mixed slurry at a certain point near the pipe discharge outlet becomes a flow where the air phase and slurry phase are very apparently separated in horizontal direction. Each single phase is often called air slug and solid-liquid slug respectively.

When a pressure sensor is attached at this point, the pressure change during the flowing of air mixed muddy slurry obtained by the sensor is made to a model form shown in **Fig. 42** (upper). The No. of pressure changing point shown here corresponds to the number shown in the flow in the actual pipe (lower in the same **Fig. 42**).

At the (2) and (7) in the **Fig. 42** (lower), if muddy slurry (solid-liquid slug) is always present between the sensor and pipe outlet, then theoretically the value of sensor will not drop to the atmospheric pressure. That is, the distance from the pipe outlet to point P_s at Mie and to point P_3 at Kumamoto is shorter than the length of one air phase in each case.

By considering the above, in the continuous records shown in Par. 4.1, the length and velocity of each solid-liquid slurry phase and air phase can be calculated by analyzing the records (P_s at Mie and P_3 at Kumamoto) of the sensor the closest to the pipe outlet.

Now, let the slurry phase be completely separated from the air phase, and let the length of one slurry phase be l_{mud}. If time t_f is one cycle time, that is, from the time when one slurry phase portion reaches the sensor to the next arrival time, then the amount of slurry Q_{tf} supplied in a period of time of t_f can be given by

$$Q_{tf} = t_f \cdot Q_s \tag{40}$$

This is also

$$Q_{tf} = A \cdot l_{mud} \tag{41}$$

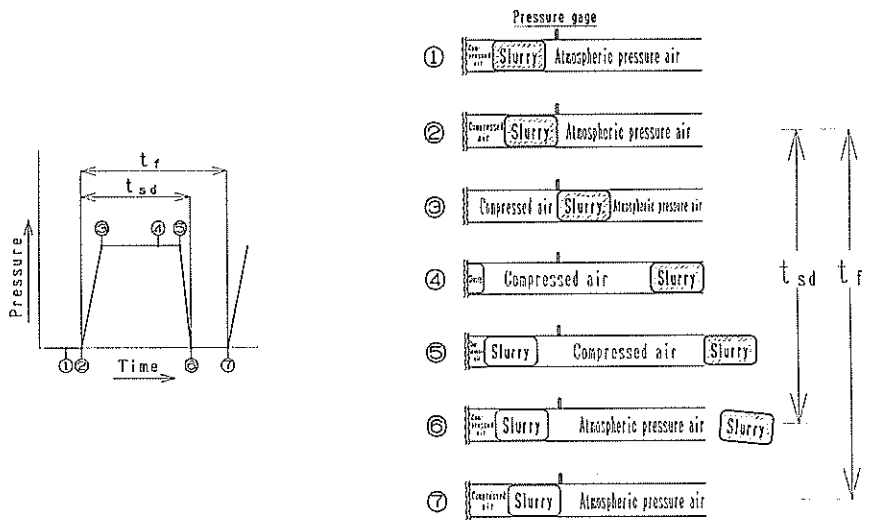

Fig. 42 Slurry flowing model for pipeline end

Therefore,

$$l_{mud} = u_s \cdot t_f \tag{42}$$

where, u_s is an apparent velocity of slurry and is defined by **Eq. 27**.

On the other hand, if the distance from the sensor to pipe outlet is l_{3d}, then this slurry will advance the distance of $l_{3d} + l_{mud}$ within a duration of t_{sd}, so that the slurry velocity v_{mud} can be calculated by

$$v_{mud} = \frac{l_{mud} + l_{3d}}{t_{sd}} \tag{43}$$

In the wave form actually obtained, uniform patterns as shown in **Fig. 42** are not always obtained. **Figures 43** and **44** show the degree of dispersion of the measured values and calculated values related to the **Eq. 42** and **43** in the form of histogram in order to show the side where an average value is located. Also, **Table 5** summarizes the mean values of the length and velocity of slurry.

With respect to Mie, the length of one slurry phase is 3~7 m in average for 4 cases, and the velocity is 8 to 13 m/s. As indicated in Par. 4.2, the velocity of slurry phase can be calculated by **Eq. 37**. This was also calculated from the conditions of construction work and the results are also shown in **Table 5**. The value for 4 cases in Mie was 7.5~11.5 m/s, and the width of no-coincidence is large when individual cases were checked. That is, as seen in the analog record of **Fig. 38** etc. there was a very difficult aspect in the case of Mie when measuring t_{sd} compared to t_f.

On the other hand, at Kumamoto, the length is 6~7 m and the velocity is 7.4~6.5 m/s for the solid-liquid slurry in two cases with different air discharge. These provide, as apparent from **Table 5**, a relatively good correlation with **Eq. 37**. In order to verify these results in Kumamoto, the discharge situation photographed by a video camera was analyzed and both the results were compared to each other. Conditions of construction at that time corresponded to the case 1, and the results of the video analysis (**Fig. 45**) indicated the mean length of 5.6 m and velocity of 11.4 m/s for solid-liquid slug. The velocity is higher compared to **Table 5** because the video data correspond to the state of the release of atmospheric pressure, the pressure inside the pipe is lower than that at sensor installation place, so that it is related to a high apparent velocity of air.

Table 5 Mean of slug length, etc.

Mie				Kumamoto					
	histogram				histogram			video	
	l_{mud} (m)	V_{mud} (m/s)	V_s (m/s)		l_{mud} (m)	V_{mud} (m/s)	V_s (m/s)	l_{mud} (m)	V_{mud} (m/s)
case 1	4.3	12.1	8.7	case 1	6.3	7.4	8.6	5.6	11.4
case 2	7.0	13.0	7.4						
case 3	5.5	9.5	5.9	case 2	7.0	6.5	7.8	——	——
case 4	2.8	7.5	11.3						

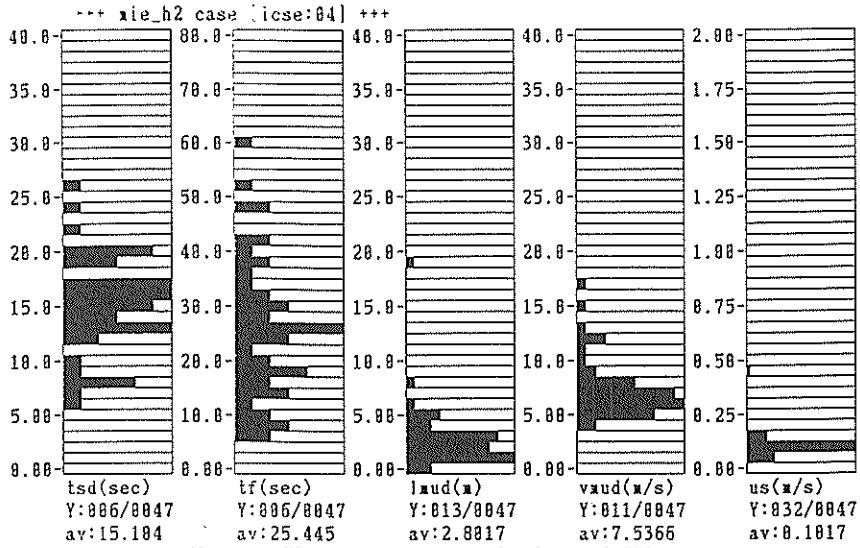

Fig. 43 Histogram for simple slug in MIE

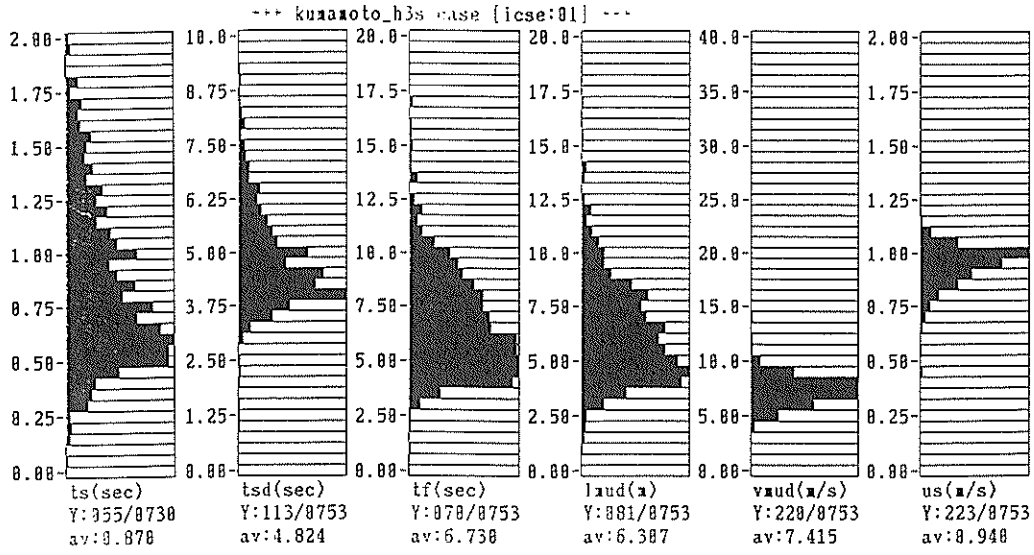

Fig. 44 Histogram for simple slug in KUMAMOTO

The same as the length of solid-liquid slurry, if the length at the discharge of air slug is l_{air}, the length of air slug can be computed by

$$l_{air} = u_{ad} \cdot t_f \tag{44}$$

where, u_{ad} is an apparent air velocity at the discharge outlet.

By the method stated above, the sum L of the length of air slug and the length of solid-liquid slug at the pipe outlet can be determined. There is an example of summarizing the non-dimensional quantity L/D using said L and pipe diameter by using

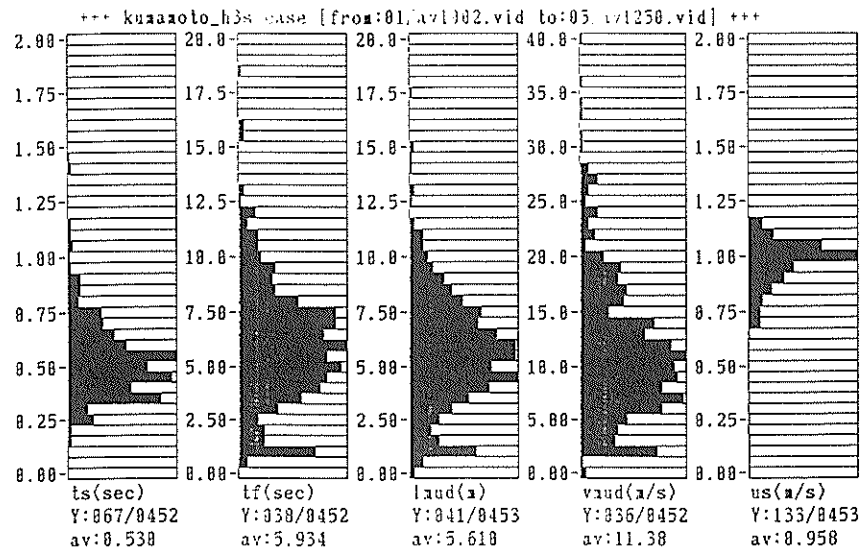

Fig. 45 Histogram of analysis video data

u_a/u_s. Whereas, this u_a can be considered the same as u_{ad} in **Eq. 44.**

Figure 46 simultaneously shows L/D calculated from laboratory experimental data, Mie data and Kumamoto data, and it can be said that they can be summarized almost in one line. That is, if slurry discharge and air discharge are given, it is possible to fairly clearly estimate the approximate length of the solid-liquid slug and air slug at the discharge outlet.

In **Fig. 46**, the mean line (dotted line) of laboratory experimental data performed in the reference No. 20 is also shown, and the data have a tendency to agree fairly well with our data.

5.3 Void Ratio in the Grown Air Mixed Flow

As seen in the continuous records of **Figs. 38** and **39**, the solid-liquid slurry phase and air phase are flowing in the form of almost complete horizontal directional separation near the pipe outlet. In this case, the void ratio in pipe is theoretically equal to the discharge ratio of air relative to the gas and solid-liquid as a whole. That is, if the air discharge ratio is X_v and void ratio is α at that position (pressure), then the following formula is valid:

$$\alpha \doteqdot X_v = \frac{u_a}{u_a + u_s} \tag{45}$$

However, as stated in Par. 5.1, the horizontal directional separation between air phase and solid-liquid slug phase is not sufficient immediately after air blowing portion, and the pressure loss is also considerably high compared to the portion near the pipe outlet.

The pressure loss per unit length of muddy slurry containing air can be expressed by **Eq. 39** as explained in Chapter 4 and by deforming this, the following formula is obtained:

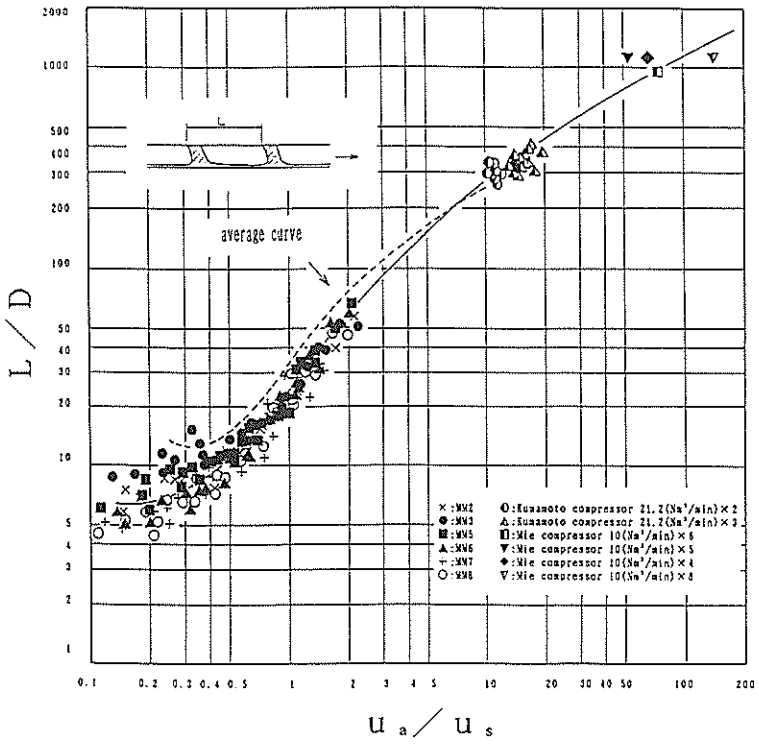

Fig. 46 Apparent velocity of air u_a/apparent velocity of slurry u_s and L/D

$$\alpha = \frac{d_{p\_s} - D_{p2}/L}{d_{p\_s} - d_{p\_a}} \tag{46}$$

Now, the pressure loss is different between the area near the air blowing portion and other portions. If the cause of the above is due to the great dependency upon the size of void ratio, then the void ratio near the air blowing portion can be computed from **Eq. 46** by using pressure loss data in the field.

Figures 47 and **48** are the graphs of the void ratio calculated by **Eq. 46** and plotted from the actual pressure loss values per unit length relative to the air discharge ratio near the sensor. **Figure 47** shows the values between P_1 and P_2 at the place the closest to air blowing portion in Mie, and **Fig. 48** shows the values for other portions where the horizontal directional separation is considered to have been grown greatly.

As understandable from **Fig. 47**, the void ratio α between the sensors P_1 and P_2 is considerably low compared to the air discharge ratio. That is, the velocity difference (slip) between the solid-liquid slug and air slug is large. Void ratio near this portion is higher than that of laboratory experimental data and is rather close to the formula shown below which is based on Nicklin's equation.

$$\alpha = 0.833 \cdot X_v \tag{47}$$

However, both the **Eq. 47** and the curve adopted in the laboratory experiments

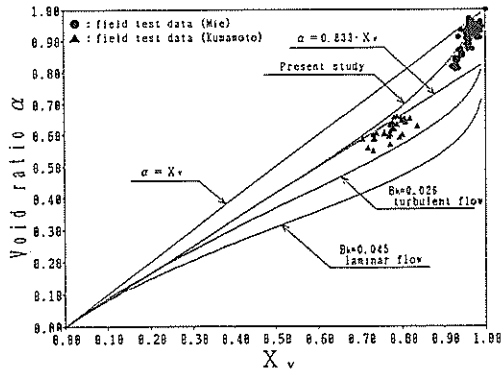

Fig. 47 Air flux ratio X_v and void rate α for field data in the vicinity of air injection part

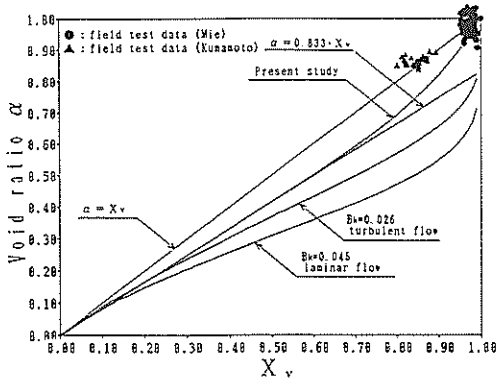

Fig. 48 Air flux ratio X_v and void rate α for field data except air injection part

have large values for X_v, and the change in the void ratio cannot be accurately expressed when their values approach to 1.

Therefore, if even a place having a high value of X_v is taken into account, then it is more realistic to adopt the **Eq. 47** in the region where X_v is low than the curve used in the laboratory experiments (the curves for laminar flow and turbulent flow in the Figure) and then to adopt a curve which will suddenly approach α = 1.0 from **Eq. 47** as X_v approaches 1. The curve shown in **Fig. 47** considering this kind of change is obtained by slightly deforming **Eq. 47**.

$$\alpha = \left(0.833 + 0.167 \cdot X_v^{7.02}\right) \cdot X_v \tag{48}$$

On the other hand, in the region where the flow is considered to be much stabilized, it can known that the void ratio is almost equal to the air discharge ratio X_v as shown in **Fig. 48**. Thus, when calculating the pressure loss of air mixed muddy slurry in an actual air pressuring plant in the field, it is better, for high accuracy, to calculate the void ratio near the air blowing portion by **Eq. 48** and thereafter to calculate with **Eq. 45**.

However, in reality, there are hardly definitive data which are able to determine the place where the horizontal directional separation will be completed for the whole length of pipe; because of this, it will be more realistic to calculate the pressure loss by using the void ratio calculated by the two methods and then to consider that the intermediate value of them as the pressure loss per unit length.

5.4 Simulation of Pressure Fluctuation in Pipe

As stated before, the pressure loss of whole air mixed muddy slurry is calculated by dividing individual loss of solid-liquid phase and gaseous phase considering each phase flows at velocity V_s proportionally with void ratio α of the point.

The following pressure loss for an actual plant is calculated with the void ratio mentioned in 5.3 at the periphery of air inlet and the other respectively.

5.4.1 Pressure Gradient in the Continuous Mixed Model

If the pressure at the upstream side with the distance equal to the length of solid-liquid slug from the pipe end is P_d, then P_d will fluctuate between the atmospheric

pressure and the pressure corresponding to the slurry flow loss per unit slug. Now, the absolute velocity at the solid-liquid slurry portion is considered as V_s and **Eq. 37** is written again below.

$$V_s = u_a + u_s \tag{49}$$

This means that the maximum pressure loss is P_d when one solid-liquid slug with the length of l_{mud} flows alone at the velocity V_s. That is,

$$P_d = \frac{4f \cdot \rho_f \cdot V_s^2 \cdot l_{mud}}{2 \cdot D} \tag{50}$$

Here, the friction loss coefficient f can be computed based on the method stated in Chapter 3.

Now, as shown in **Fig. 49**, the distance from the air blowing portion to pipe end is Lt, and the relation between the pressure in pipe, P_{n-1}, at certain points taken toward the upstream every Δl from the pipe end and the pressure in pipe, P_n, at the points one section apart can be obtained by

$$P_n = P_{n-1} + \left\{ d_{p-s} \cdot (1-\alpha) + d_{p-a} \cdot \alpha \right\} \cdot \Delta l \tag{51}$$

where, if l_{mud} is adequately small, then the average void ratio between P_n and P_{n-1} can be substituted by the average void ratio in preceding section. However, in the computation of P_1, calculation is to be made by using the point P_0, that is, the void ratio obtained for pressure P_d.

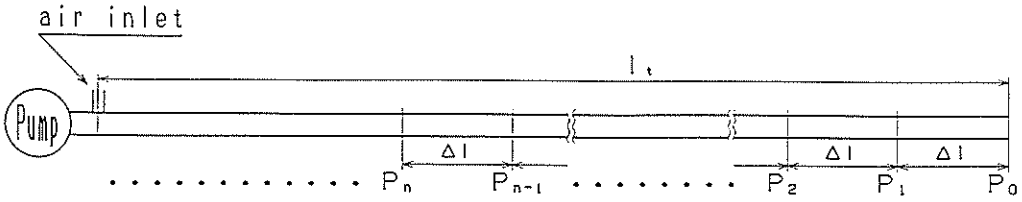

Fig. 49 Schematic diagram of pipline partition for simulation

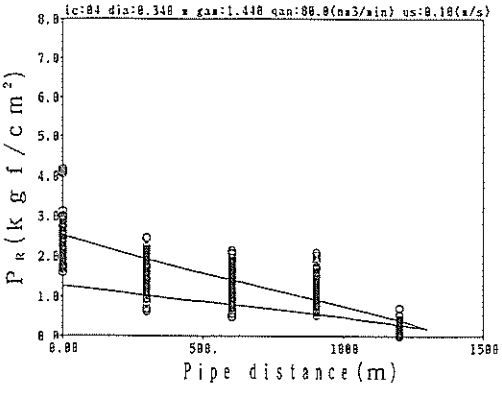

Fig. 50 Calculation of pressure gradient and field data (MIE case 4)

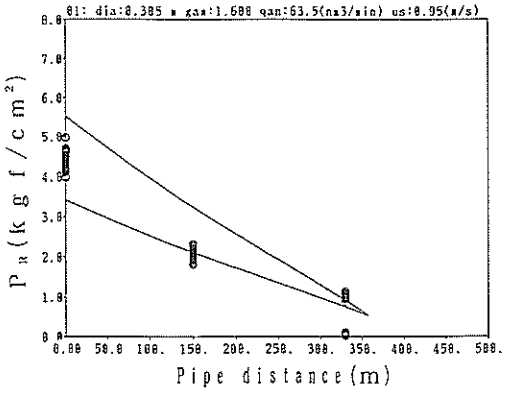

Fig. 51 Calculation of pressure gradient and field data (KUMAMOTO case 1)

Figures 50 and **51** show the calculations of void ratio made over the whole length for the single solid-liquid slurry length Δl from the field data obtained by using **Eqs. 45** and **48**. Here, Δl is 50 m for Mie and 20 m for Kumamoto. For l_{mud}, the mean value of histogram of **Table 5** is used.

By plotting field data on this diagram, it can be known that they are between the calculated values for void ratio in both cases of Mie and Kumamoto. As explained previously, in principle, it is valid to use the void ratio of **Eq. 48** near the air blowing portion and then to shift smoothly to the results using the void ratio of **Eq. 45**. In reality, however, the transition points for both of them have not been fully clarified and thus it is better to use the value as estimate which is pinched by both the curves.

5.4.2 Pressure Gradient in the Complete Horizontal Directional Separation Model

Pipe pressure change curve obtained in Par. 5.4.1 is for an arbitrary portion of the whole length of pipe and is a simulation with the mixing of a certain proportion of air phase and solid-liquid slurry phase as prerequisite. Therefore, if the pressure at one point is checked, only the mean value always having no fluctuation can be obtained.

However, in the horizontal directional separation flow developed in actual horizontal pipe, the pressure gradient is significant only in the solid-liquid slurry phase, and there will be almost no pressure gradient in horizontal direction in air phase. By performing a simulation based on the above presumption, the pressure fluctuation obtained at a certain point in pipe by the simulation will be more realistic.

In this simulating calculations, one cycle is from time zero when the tip of some solid-liquid slurry reaches the pipe outlet to the time when subsequent solid-liquid slurry phase again reaches the pipe end, and pressure distribution is calculated over the whole pipe length every certain period of time.

For instance, some examples of the situation of several flows in one cycle and the state of pressure distribution at that time are as shown in **Fig. 52**. After the state (3), the pressure distribution state of (1) occurs again. Therefore, if a pressure sensor is placed on a line indicated by A-A, them, in the time series data on the line, a pressure change similar to a trapezoid will be recorded.

In the calculations of pressure distribution over the whole length of pipe at each time, the absolute velocity of solid-liquid slug is determined from an apparent velocity of slurry and air at the pipe end, that is, in the state opened to the atmosphere; and then pressure loss over the slurry length l_{mud} from pipe end is computed. That is, P_1 can be computed in (1) of **Fig. 52**. Then, the apparent velocity of air at pressure P_1 is determined, and then void ratio at this point is computed from said velocity and the apparent velocity of slurry. From this, air slug length lair can be determined. Thus, l_2, P_2 can be determined from the following equation:

$$P_2 = P_1 \tag{52}$$

In this way, the distance from pipe end and pressure in pipe at a certain time can be determined. At the time ((3) of **Fig. 51**) when single solid-liquid slug originally considered has disappeared at pipe end, the pipe end is in the state opened to the atmosphere, so that computation is to be made by using the following formula:

$$P_1 = P_o = P_{at} \tag{53}$$

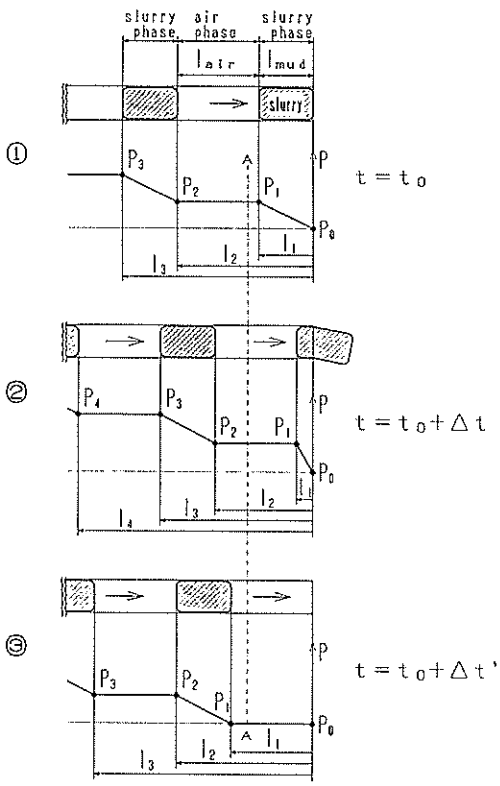

Fig. 52 Model of simulate calculation for horizontal direction perfectly separation flow

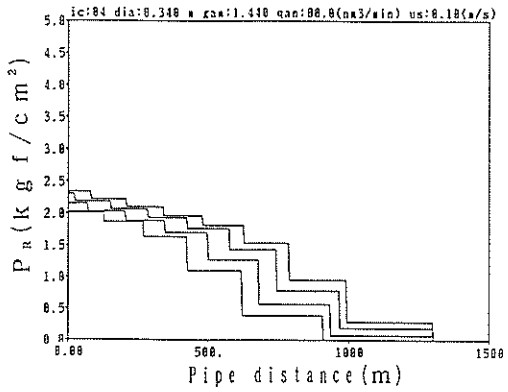

Fig. 53 Calculation of pressure gradient For horizontal direction perfectly separation flow (MIE case 4)

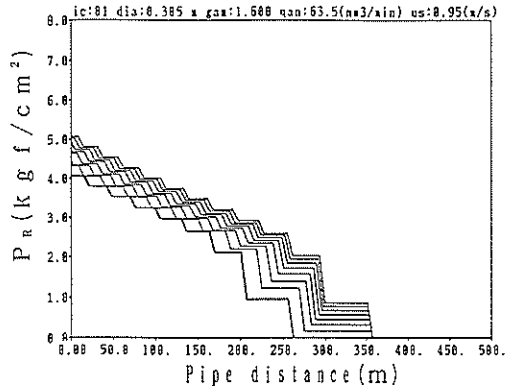

Fig. 53 Calculation result of pressure gradient for horizontal direction perfectly separation flow (KUMAMOTO case 1)

where, P_{at} is atmospheric pressure.

Figure 53 is a calculation example for Mie data, in which the solid-liquid slug length l_{mud} is used as the mean value of the histogram shown in **Table 5**, and one cycle is shown every 50 millisec.

In the same manner, **Fig. 54** shows the results for Kumamoto data. It can be known that Mie data show the length of air phase extremely larger than the length of slurry phase compared to Kumamoto.

At the plant in the field, pressure sensors are attached at certain positions in the direction of length. For instance, in the case of Mie, five pressure sensors P_1~P_5 are attached and three sensors in Kumamoto.

Pressure fluctuation obtained at these positions is indicated on time axis, and the simulation results and Mie data (Case 4) are compared in **Fig. 55**. However, in the case of Mie, three points P_1, P_3 and P_5 are taken and compared to avoid complication.

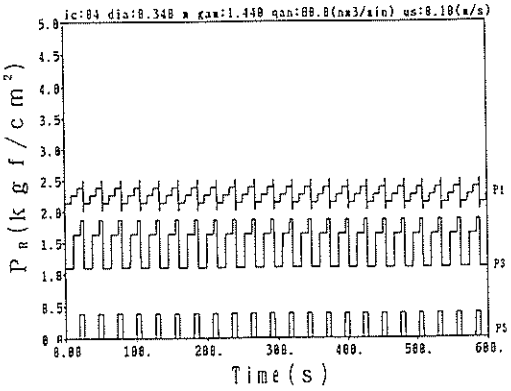

Fig. 55 Calculation result of pressure variation for horizontal direction perfectly separation flow (MIE case 4)

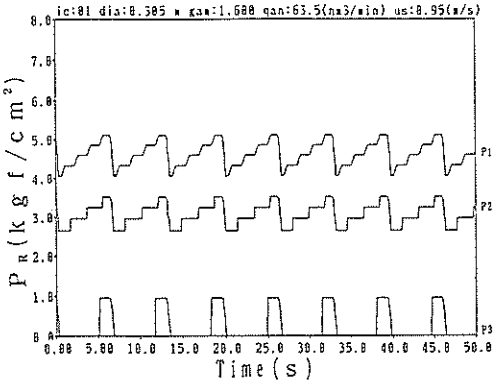

Fig. 56 Calculation result of pressure variation for horizontal direction perfectly separation flow (KUMAMOTO case 1)

Results of this simulation show many portions agreeing with each other fairly well. That is, it can be presumed that the situation of flow of air mixed muddy slurry in pipe at these sensors is close to a flow having a complete horizontal directional separation.

However, by examining the pressure fluctuation at the air blowing portion such as P_1, it can be known that the width of fluctuation in actual data is small and horizontal directional separation at this portion is still incomplete. This kind of situation is also the same in Kumamoto (refer to **Fig. 56** and case 1).

The contents stated above indicate that, if pressure sensors are attached to adequate positions at a pipe end in the operation control of an actual transport plant compressed by air, then the length, pitch and others of single slurry can be obtained from that data and these values have validity. Also, by the simulation method using these data, the situation of flowing through the whole pipe can be mostly presumed from these sensors at the pipe end. This will greatly contribute to the automatic operation of the construction works.

5.5 Theoretical Transport efficiency in Actual Plant

Conventionally, in the air compressed method for this kind of horizontal pipe, the review of its transport efficiency was hardly tried. Probably because the theoretical estimation of energy required for the transport without air is not easy since this method is possible only by using air.

This time, we have successfully obtained the theoretical energy required for transporting slurry without air though this kind of transport is impossible in actual pipeline transport. Therefore, we calculated the theoretical efficiency in the form of the ratio to air supply energy for the above.

Now, if the specific weight of slurry is γ_s and the theoretical power required for transporting the slurry at discharge Q_s for a certain distance is P_{sreq}, then the said power can be given by

$$P_{sreq} = \frac{\gamma_f \cdot Q_s \cdot H_s}{75} \tag{54}$$

where, head H_s can be expressed as follows by using the required discharge pressure P_{req} of slurry pump:

$$H_s = \frac{\gamma_w}{\gamma_f} \cdot \left(P_{req} \times 10\right) \tag{55}$$

In this case, the required discharge pressure is converted into the height of water column, and it is further converted into the height of mud water. Here, γ_w is the specific weight of fresh water and P_{req} is expressed in kgf/cm^2.

On the other hand, if air is assumed to be supplied at P_1 to the slurry line, then energy required for pressuring up to P_1 by a compressor can be calculated by the following formula based on isothermal compression in compressing process:

$$P_{sin} = \frac{G_a \cdot P_{at} \cdot v_0 \cdot ln\left(\dfrac{P_1}{P_{at}}\right)}{75} \tag{56}$$

Here, G_a is the amount of air supply (kg/s) and P_{at}, v_0 are absolute pressure (kgf/m^2) and specific volume (m^3/kg) under the state of atmospheric pressure.

Now, the compression energy of air and the energy required for transportation without slurry air are determined, then the theoretical efficiency η of the slurry transport plant with compressed air is given by

$$\eta = \left(\frac{P_{sreq}}{P_{sin}}\right) \tag{57}$$

Table 6 shows the theoretical efficiency determined from **Eq. 57** under the transport conditions in Mie and Kumamoto. Values of η for apparent discharge ratio u_s/u_a for slurry and air plotted in **Fig. 57**. However, u_a is the value for standard state.

As far as the above indicates, the field data obtained this time the influence of u_s/u_a is not indicated with respect to η, and the average efficiency is considered to be about 30~40%. From the meaning of the efficiency as absolute value, the trial this time merely gives a theoretical efficiency but this value will be sufficiently useful for comparing various plants with each other.

Table 6 Theoretical efficiency

	Mie				Kumamoto	
case	case1	case2	case3	case4	case1	case2
Qan(Nm^3/min)	60	50	40	80	63.6	42.4
us(m/s)	0.152	0.176	0.104	0.092	0.942	0.842
us/ua	0.013	0.019	0.014	0.006	0.062	0.087
Preq(kgf/cm^2)	37.179	37.621	37.917	37.387	9.123	8.878
Psin(kw)	163.740	135.480	78.160	161.930	178.290	121.200
Psreq(kw)	50.220	58.860	35.050	30.570	61.750	53.380
efficiency η (%)	30.67	43.45	44.84	18.88	34.63	44.04

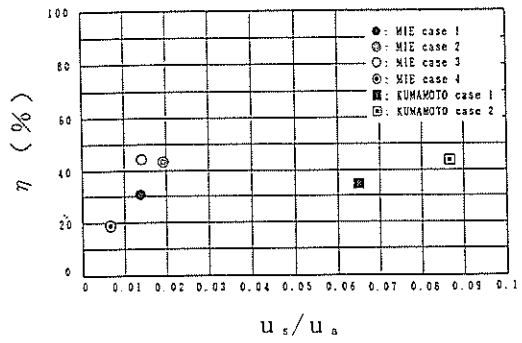

Fig. 57 Apparent velocity of slurry u_s/apparent velocity of air u_a and theoretical efficiency

6. Conclusions

After we performed the laboratory flow experiment of muddy slurry with compressed air in horizontal pipe and measuring work in actual plant. Various points are clarified about fluidity of solid-liquid slurry and the fluidity of muddy slurry with compressed air.

They are summarized hereinafter.

(1) With respect to the flow of solid-liquid slurry itself through pipe, a power law model using Metzner-Reed's Reynolds number was used for Mie data, and a Bingham fluid model for Kumamoto data. These rheology constants were estimated from the laboratory transport data for the same slurry with pipe diameter of 40~80 mm but can be sufficiently applied also to the pipeline in the field with the pipe diameter greater than 300 mm.

(2) The mean void ratio of laboratory test in pipe can be measured directly by the change of the hopper level. The decrease rate of void ratio against the air discharge ratio X_v is greater in laminar portion than in turbulent portion. This is caused by the difference of velocity distribution between laminar flow and turbulent flow. The coefficients of B_k in **Eq. 29** of Inoue et al., derived from the measured void ratio are 0.045 for laminar flow and 0.026 for turbulent flow.

(3) The pressure loss of air mixed flow is greater in fresh water and muddy slurry of low density than in non-air flow without exception. However, when the density becomes higher, it appears to be lowering its pressure loss as compared with non-air flow at some velocity range. Fluidity characteristics of air mixed flow can be explained fairly clearly by horizontal directional separation model shown in this paper.

(4) According to the method mentioned in (3), the lowest pressure loss point appears when the mean velocity of air mixed slurry comes off laminar flow. Thus, we can obtain the optimum slurry arranging method against the constant air discharge or the optimum air mixture ratio against the constant density slurry.

(5) Air mixing ratio in the slurry transport method with compressed air in the field is extremely high compared to ordinary air liquid flow. Thus, in estimating the void ratio in this range, we formulated a new equation based on the conventional calculating formula for void ratio. This is a curve suited to the calculated void ratio when the pressure loss of air mixed slurry is assumed to follow the method described in Par. 4.3. And this can be used when estimating void ratio near the

air blowing portion especially in the air compressed transport plant.

(6) Pressure inside the pipe suddenly decreases in a certain section immediately after air mixing. Thereafter, the lowering tendency slowed down. By considering the change in void ratio in pipe, the air phase and solid-liquid slurry phase are not fully separated in horizontal direction for a certain period of time after mixing air and, because of this, the void ratio decreased below the air liquid mixing ratio (slip of air phase and solid-liquid slurry phase is large) but the horizontal directional separation gradually progresses and the void ratio became equal to the air liquid mixing ratio. This seems to be the main cause of the great pressure loss immediately after mixing air.

(7) Pressure loss when air is mixed can be calculated by using the horizontal directional separation model. After the point where the air slug and solid-liquid slug are considered to be separated horizontal directionally, the air mixing ratio can be replaced by using void ratio in the calculation. But the data agree much better when the void ratio stated in (5) is used near the air mixing portion. Prediction for the location where the horizontal directional separation will be completed is difficult. Thus, it is more realistic to estimate the pressure loss from an intermediate value calculated from the two methods.

(8) By the method explained in this report, it is possible to calculate the pressure gradient for the whole length of a pipe containing only the solid-liquid slurry without containing air. Energy required for the above flow is given by the compressed air by our assumption, and then we calculated the theoretical efficiency. As a result, the efficiency was 30~40% for both Mie and Kumamoto.

(9) Length of air slug, solid-liquid slug and its generating pitch can be assumed by the methods explained in this report if u_a/u_s at atmospheric state is known. And it is possible to predict an air mixed flow expected to be realized in a designed plant fairly well.

7. Postscript

In this report, we analyzed the laboratory flow experimental data and the working data of air mixed slurry transport plant in the field. Even though there are still some insufficient points, for realizing the design with more appropriate slurry transport conditions for various flows, it seems to be necessary to further collect field data with diversified scales of slurry transport and soil conditions and to apply and review the methods obtained this time to these conditions.

In collecting the field data this time, the Toyo Construction Co., Ltd. gave us its cooperation in various phases, with whom we conducted joint research for many years on the high-efficiency dredging and transporting system utilizing air. Particularly, the Mie data were collected by the said Company and analyzed by the Port and Harbor Research Institute.

In addition, in the field measurement work in the Kumamoto Port, the staff of the Kumamoto Port Construction Office and Shimonoseki Machinery Office, 4th Construction Bureau gave us their cooperation.

We would like to express our deepest gratitude to those concerned with the above activities.

(Reveived on August 31, 1992)

References

1) OKAYAMA, Y. and YAGI, T.,: Air-lift in dredging (in Japanese), *Proceeding of 1977 Annual Research Presentation of PHRI*, pp. 205~235, Dec. 1977.
2) USAMI, T., SAITO, T. and KITAHARA, R.,: Lifting Characteristics of Solid by Air Lift Pump (2nd Report) (in Japanese), *Journal of the Mining and Metallurgical Institute of Japan*, Vol. 98, No. 1127, pp. 29~34, Jan. 1982.
3) SAITO J. and others: Experiment on Earth-pressured Shield Tunnelling to Increase Fluidity of Excavated Soil by Mixing Bubbles into Pressurized Chamber (in Japanese), *Report of the Technical Research Institute OHBAYASHI-GUMI, LTD.* No. 21, pp. 105~109, 1980.
4) SATIO, J. and others: Experiments on Continuous Transportation of Excavated Soils in Foam-injected Shield Tunnelling (in Japanese), *Report of the Technical Research Institute OHBAYASHI-GUMI, LTD.* No. 27, pp. 107~111, 1983.
5) KURIHARA, K.: Transportation of Muck by Wind Force (in Japanese), *Journal of Civil Engineering Construction*, Vol. 20, No. 4, pp. 26~35, April 1980.
6) FUJII, K. and OHTSU, F.,: Remove of accumulated organic material by Uzer-pump Dredger (in Japanese), *Summary Report of Port and Harbor Technology*, No. 100, pp. 172~197, March 1987.
7) CHHABRA, R.P., et al.,: Co-current Flow of Air and Shear Thinning Suspensions in Pipes of Large Diameter, *Chem. Eng. Res. Des.*, Vol. 61, pp. 56~61, Jan. 1983.
8) CHHABRA, R.P., et al.,: Isothermal Two-Phase Flow of Air and Aqueous Polymer Solutions in A Smooth Horizontal Pipe, *Chem. Eng. Res. Des.*, Vol. 62, pp. 22~32, Jan. 1984.
9) OKAYAMA, Y., AYUGAI, M., SUZUKI, M. and FUKUMOTO, H.,: Fluidity Characteristics of Muddy Slurry with Compressed Air in Horizontal Pipe (in Japanese), *Report of PHRI*, Vol. 30, No. 2, pp. 533~557, June 1991.
10) MINE, H.,: Dredging and Reclamation Work in Kumamoto Port by the Method of High Density Transport with Compressed Air (in Japanese), *Marine Voice 21*, No. 164, pp. 35~44, 1992.
11) GOVIER, G.W. and AZIZ, K.,: The Flow of Complex Mixtures in Pipes, *Van Nostrand Reinhold Company*, NY. 1972.
12) METZNER, A.B. and REED, J.C.,: Flow of Non-Newtonian Fluids-Correlation of the Laminar, Transition, and Turbulent-Flow Regions, *A.I. Ch. E. Journal*, Vol. 1 No. 4, pp. 343~440, December 1955.
13) MASUYAMA, T. and KAWASHIMA, T.,: On Lower Critical Reynolds Number of Non-Newtonian Fluid Flow (in Japanese), *Transactions of the Japan Society of Mechanical Engineers*, Vol. 43, No. 373, pp. 3320~3326, Sep. 1977.
14) RYAN, N.W. and JOHNSON, M.M.,: Transition from Laminar to Turbulent Flow in Pipes, *A.I. Ch. E. Journal*, Vol. 5 No. 4, pp. 433~435, December 1959.
15) KEMBLOWSKI, Z. and KOLODZIEJSKI, J.,: Flow resistance of non-Newtonian fluids in transition and turbulent flow, *International Chemical Engineering*, Vol. 13, No. 2, pp. 265~279, April 1973.
16) TSURUYA, H.,: Investigation of Rheological Properties of Soft Muds with a Rotary Visco-meter (in Japanese), *Technical Note of PHRI*, No. 566, pp. 1~29, Dec. 1986.
17) INOUE, A. and AOKI, S.,: Fundamental Studies on Pressure Drop in Air-Water Two-Phase Flow in Vertical Pipes (4th Report) (in Japanese), *Transactions of the*

Japan Society of Mechanical Engineers, Vol. 36, No. 288, pp. 1366~1373, August 1970.

18) SEKOGUCHI, K. and others: Development of Heat Transfer (Vol. 1), *Yokendo*; 1973.

19) OKAYAMA, Y. and others: The Study on the Effect of Air Injection for Vertical Slurry Transport (in Japanese), *Technical Note of PHRI*, No. 656, pp. 1~38, Sept. 1989.

20) SEKOGUCHI, K., SATO, Y. and KARIYASAKI, A.,: On the Disturbed Flow Regions in Horizontal Two-Phase Air-Water Flow (in Japanese), *Transactions of the Japan Society of Mechanical Engineers*, Vol. 35., No. 279, pp. 2234~2242, Nov. 1969.

List of Symbols

A : cross sectional area of pipe
a : specific plug radius
D : pipe diameter
D_p/L : pressure loss per unit length
D_{p2}/L : pressure loss per unit length of slurry containing air
d_{p_a} : pressure loss per unit length when gaseous phase is flowing at absolute velocity V_a
d_{p_as} : pressure loss per unit length when only air is assumed to be flowed
d_{p_mix} : pressure loss per unit length of air mixed slurry divided by void ratio
d_{p_s} : pressure loss per unit length when only solid-liquid phase is flowing at absolute velocity V_s
d_{p_ss} : pressure loss per unit length when only transport slurry is assumed to be flowed
f : Fanning's pipe friction loss coefficient
f_{bt} : Tomita's friction loss coefficient for Bingham fluid
f_c : friction loss coefficient at critical Reynolds number
f_w : Fanning's friction loss coefficient
H_s : discharge head of pump (high of mud water)
K : consisyency coefficient
L : $l_{air} + l_{mud}$
l_a : length of air slug
l_{air} : length of one air slug
l_{mud} : length of one solid-liquid slug
l_s : length of liquid slug
l_z : $l_a + l_s$
n : rheology index
$P_{o\ldots n}$: pressure inside pipe, position of pressure gauge
P_{sin} : supplied power
P_{sreq} : required power
Q_a : amount of air supplied per unit time
Q_s : amount of liquid or solid-liquid slurry flowing per unit time
r : radius from the center of pipe
r_o : radius of pipe
R_{ebt} : Tomita's Reynolds number
R_{el} : Reynolds number
R_{eMR} : Metzner-Reed's Reynolds number
R_{eMRC} : critical Reynolds number
S_v : shear rate

u : velocity in pipe
u_a : apparent air velocity
u_s : apparent velocity of liquid or solid-liquid slurry
V_a : absolute velocity of air slug
V_f : absolute velocity of liquid below air slug
V_s : absolute velocity of liquid slug portion
X_v : air discharge ratio
α : void ratio
α_r : void ratio considered from the center of pipe in the radius direction
γ_f : specific weight of slurry
γ_w : specific weight of clear water
η : theoretical efficiency of the slurry transport plant with compressed air
μ_B : viscosity coefficient of Bingham fluid
μ_w : viscosity coefficient of clear water
ρ_a : density of air
ρ_f : density of liquid or slurry
ρ_w : density of clear water
τ : shear stress
τ_o : shear stress at pipe wall (r_0)
τ_y : yield stress of Bingham fluid